EXPLORING SIGNALING PATHWAYS IN HIGHLY METASTATIC CANCERS

By
Gabriella Russo

A thesis submitted to the Johns Hopkins University in conformity with the requirements for the degree of Masters of Science in Engineering

Baltimore, Maryland

May 2018

Abstract

Metastasis, the spread of cancer from a primary site to distal sites throughout the body, is responsible for 90% of all cancer related deaths.[1] Current development of anti-cancer therapeutics assumes that drugs targeting tumor growth will also influence metastasis, or that interrupting metastasis in the face of overwhelming tumor growth inhibition is not necessary. However, proliferation-targeted therapies have little efficacy in targeting or slowing metastatic cellular migration and patients succumb to their disease due to advanced metastasis, not due to tumor growth.

Triple negative breast cancer (TNBC) and pancreatic ductal adenocarcinoma (PDAC) are two of the most metastatic cancer subtypes. Currently, there are no targeted therapies available for TNBC, but for estrogen receptor (ER), progesterone (PR), and HER2 subtypes, there are highly successful therapies available to patients.[2] The lack of targeted therapies correlates with the worse prognosis associated with TNBC, which has a five-year survival rate of 77% compared to 93% for other subtypes of breast cancer.[3] For PDAC, the five-year survival rate is 5% for distant disease, which has not improved since 2005 and for localized disease, the five-year survival rate is less than 30% which is extremely low compared to other cancer types.[4]

A new paracrine signaling pathway was discovered that infers a strategy to inhibit cancer cell migration by exploiting the synergistic signaling between interleukin 6 (IL-6) and interleukin 8 (IL-8).[5] The discovery of this pathway was facilitated by three-dimensional (3D) models specifically designed to track cellular migration in a collagen-rich tumor microenvironment. It is important to note this effect is specific to metastatic cancers, making the inhibition of IL-6 and IL-8 receptors a strategy to slow migration of highly metastatic cancers.

This study further explores one of the highly metastatic cancer cell lines, MDA-MB-231, and the impact of E-cadherin on both proliferation and the invasive phenotype of these cells. We also studied the role of IL-6 and IL-8 signaling in PDAC and discovered the combination of anti-metastatic treatment (tocilizumab and reparixin) with a current monotherapy (gemcitabine) for PDAC significantly decreased tumor size and metastasis in a patient derived xenograft mouse model.

Thesis Advisor: Dr. Denis Wirtz

Thesis Committee/Reader: Dr. Jonathan Hernandez

Acknowledgements

The work documented in this thesis would not have been possible without the guidance and encouragement from my family and friends. I would like to start by thanking my mother for always supporting me and believing in me. I would not be the person I am today without her love and support. She has taught me how to be a strong, independent woman and I cannot thank her enough for all she has given me.

I would also like to thank Dr. Denis Wirtz for welcoming me into his lab as an undergraduate researcher my freshman year and giving me the guidance and opportunities throughout my undergraduate career. His enthusiasm for research is contagious, which is one of the many reasons I am going to continue my research career next semester as I begin my Ph.D.

I would like to thank all of the Wirtz Lab members for their help and day-to-day collaborations, especially my two mentors for the projects presented in this thesis – Dr. MengHorng Lee and Michelle Karl, a second year Ph.D student. I have had the pleasure of working with Dr. MengHorng Lee for the past two years and cannot thank him enough for all his guidance and support as I prepared this thesis. I have also had the pleasure of working closely with Michelle Karl since she joined the lab a year and a half ago. Her dedication to research and eagerness in exploring new projects is inspiring, and I am so very lucky to work with her.

I would also like to thank Dr. Jonathan Hernandez from the NIH for sitting on my thesis committee and supporting me through this process. He has been instrumental in my research career, and I am very much so looking forward to working with him during my PhD.

And a very special thank you to Dr. Hasini Jayatilaka, who has been an inspiration to me since I first met her in the Wirtz Lab in November 2013 and has been an amazing mentor throughout my masters thesis. Without her guidance and support, I would not be the researcher I am today. I am forever grateful for all her help and encouragement, and I am looking forward to our future collaborations.

Lastly, a huge thank you to all my friends and professors at Johns Hopkins, who have been a part of this journey. Thank you to all my friends for making me laugh through the toughest of times. You are some of the most amazing people I have met, and I cannot wait to see what you all accomplish – especially Joseph Federico, Kristen Manto, Mitchell Keller. To my professors, thank you for making me think critically and grow as a student – very special thanks to Dr. Lise Dahuron and Dr. An Goffin.

TABLE OF CONTENTS

Abstract ii

Acknowledgements iii

LIST OF TABLES vi

LIST OF FIGURES vi

1 Metastasis 1

1.1 Background 1

1.2 Highly metastatic cancers 1

1.3 Mechanism of metastasis 2

1.4 Single cell migration through a collagen I matrix 3

1.5 Motivation for the study 4

2 Migratory phenotypes 5

2.1 Mechanism of cell-density dependent migration in TNBC 5

2.2 Targeting IL-6 and IL-8 to slow metastasis 7

2.2.1 Tocilizumab and reparixin – mechanism of action 7

2.2.2 Impact of tocilizumab and reparixin combination therapy on metastatic burden 8

2.3 Impact of E-cadherin on migratory phenotype 9

2.3.1 E-cadherin: the tumor suppressor gene 9

2.3.2 Paradox of E-cadherin 10

2.3.3 Impact of E-cadherin on TNBC 12

3 A novel spheroid model to study migratory phenotypes in TNBC 14

3.1 Double-layered spheroid model (3DLTS) 14

3.2 How E-cadherin affects invasive phenotype 15

3.2.1 MAPKinase signaling pathway and the role of ERK, JNK, p38 16

3.2.2 WNT signaling pathway and the role of beta-catenin 16

3.2.3 HIPPO signaling pathway and the role of YAP/TAZ 17
3.3 RT-PCR to evaluate signaling pathways 17
3.3.1 PCR Results- MAPKinase signaling pathway 18
3.3.2 PCR Results- WNT signaling pathway 19
3.3.3 PCR Results- HIPPO signaling pathway 19
3.4 Exploring ERK at the protein level 20
3.5 Drug inhibitor studies using 3DLTS 21
3.5.1 Drug screening with MAPKinase and WNT inhibitors 21
3.5.2 MEK inhibitor impact on invasive phenotype 23
3.6 Future directions 25
4 Pancreatic ductal adenocarcinoma and IL-6/IL-8 signaling 25
4.1 Background 25
4.2 Standard of care therapies 26
4.3 Impact of cell-density on secreted IL-6/IL-8 in PDAC 28
4.4 *In vivo* study – patient derived xenograft (PDX) mouse model 29
4.4.1 Experimental design of *in vivo* study 29
4.4.2 Results of *in vivo* study 30
4.5 Future studies 33
5 Exploring unconventional metastasis 33
5.1 Metastasis and the omentum 33
5.2 Development of a novel co-culture system 34
5.3 Future studies 35
6 Materials and methods 35
7 Supplementary figures and data 44

LIST OF TABLES

Table 1: Inhibitors used for drug screening. 21

Table 2: PDX mouse model treatment groups and dosages for each group. 30

LIST OF FIGURES

Figure 1: Metastasis cascade 2

Figure 2: Cell-density effect on IL-6 and IL-8 secretions 6

Figure 3: Cascade initiated by IL-6 and IL-8 6

Figure 4: Mechanism of action for tocilizumab and reparixin 8

Figure 5: Impact of tocilizumab and reparixin on tumor volume and metastatic burden 9

Figure 6: Schematic overview of E-cadherin-catenin complex 10

Figure 7: Schematic of the genes analyzed 11

Figure 8: Recurrence probability for patients expressing E-cadherin 12

Figure 9: Normalized spheroid volume over time 13

Figure 10: Tumor volume over time for in vivo study 13

Figure 11: Spheroid progression differences seen in over-expression of E-cadherin 15

Figure 12: Invasive phenotype induced by E-cadherin over-expression 15

Figure 13: Relative expression of CDH1 in 2D and 3D conditions 18

Figure 14: Relative Gene Expression of MAPKinase Signaling 18

Figure 15: Relative gene expression of WNT signaling pathway 19

Figure 16: Relative gene expression of HIPPO signaling pathway 20

Figure 17: Protein Expression of ERK and Phosphorylated-ERK are higher in MDA-MB-231 + E-cadherin 3DLTS 21

Figure 18: Visualization of inhibitor impact on 3DLTS (MDA-MB-231 + E-cadherin). 22

Figure 19: 10uM inhibitor screening with MDA-MB-231+E-cadherin 3DLTS 23

Figure 20: IC_{50} graphs of MI4 for both the inner spheroid volume 24

Figure 21: Reversion of invasive phenotype with MEK inhibitor treatment 24

Figure 22: Gemcitabine - Primary mechanism of action 26
Figure 23: Gemcitabine- secondary mechanism of action 26
Figure 24: 5-Fluoruoracil- Mechanism of action 27
Figure 25: 5-FU-mechanism of action 28
Figure 26: Concentration of secreted IL-6 and IL-8 increase with cell density in Capan-1 29
Figure 27: Comparison of tumor growth for each condition 31
Figure 28: Final tumor measurements for PDX mouse model 31
Figure 29: Excised tumors for each treatment group. 32
Figure 30: Metastatic burden to lung and liver is reduced in T+R+G combination group. 32
Figure 31: Omentum co-culture system. 34

1 Metastasis

1.1 Background

Metastasis is responsible for 90% of cancer related deaths, yet it is not the primary focus of anticancer therapies.[1] Metastasis is the spread of cancer cells from the primary tumor site to distal site(s) via the vascular and lymphatic systems. Proliferation and migration are two key drivers of metastasis, but current therapies primarily aim to address the highly proliferative nature of cancer cells. For example, both therapies currently used to treat PDAC, a highly metastatic cancer, are cytotoxic and have not been shown to effectively treat metastasis.[6] Typically, it is not the size or rapid growth of the primary tumor that kills patients, but rather the migration of cells from the primary tumor to distal sites.[4] Cellular migration is not a consequence of proliferation and should be considered a completely separate mechanism. Indeed, pharmacological agents that target proliferation do not have an impact on cell migration and can actually make cells more migratory. This study explores the mechanisms that govern cell migration and identifies potential therapeutics for triple negative breast cancer and pancreatic ductal adenocarcinoma, which are classified as highly metastatic.

1.2 Highly metastatic cancers – triple negative breast cancer and pancreatic ductal adenocarcinoma

In this study, we explore two highly metastatic cancers: triple negative breast cancer (TNBC) and pancreatic ductal adenocarcinoma (PDAC). There has been little improvement in outcomes for these two diseases because current therapies for these types of cancers cannot effectively target metastasis.[4] It is assumed that pharmacological agents that can target tumor growth can also target metastasis, so many of the current treatments for cancers were primarily tested for their anti-proliferative capability but were not tested for anti-metastatic capability.[4] Therefore, most cytotoxic drugs are effective in targeting proliferation but have no effect on preventing metastases.[4] Currently, there are no targeted therapies available to treat TNBC, but there are highly successful therapies available for the other subtypes of breast cancer.

Due to the lack of specific therapies for TNBC, patients diagnosed with TNBC have a significantly worse prognosis when compared to other subtypes of breast cancer; TNBC has a five-

year survival rate of 77% compared to other subtypes of breast cancer which have a 93% five-year survival rate.[3] Patients diagnosed with TNBC also tend to be younger when compared to other breast cancer subtypes.[3] For PDAC, the five-year survival rate is 5% for distant disease and 30% for localized disease, which has not improved much over the past decade. These five-year survival rates are some of the lowest among all other types of cancer.[4]

1.3 Mechanism of metastasis

The spread of cancer to multiple sites results in patients having a higher risk of succumbing to their disease or a higher risk of recurrence. If a tumor can be isolated and localized to a single site, resection surgeries to remove the entirety of the cancer can be performed and fewer cycles of chemotherapy would be needed to achieve remission. Localized disease in breast cancer has over a 90% chance of 5-year survival and in pancreatic cancer, localized disease is the only stage in which the 5-year survival percentage has increased significantly in the last decade.[4]

In order to effectively treat highly metastatic cancers, the mechanism of metastasis needs to be further elucidated. Depicted in Figure 1, the metastasis cascade is a complex process, with multiple steps regulated by genetics, the external environment, cellular signaling, and physical interactions within the tumor microenvironment.[7]

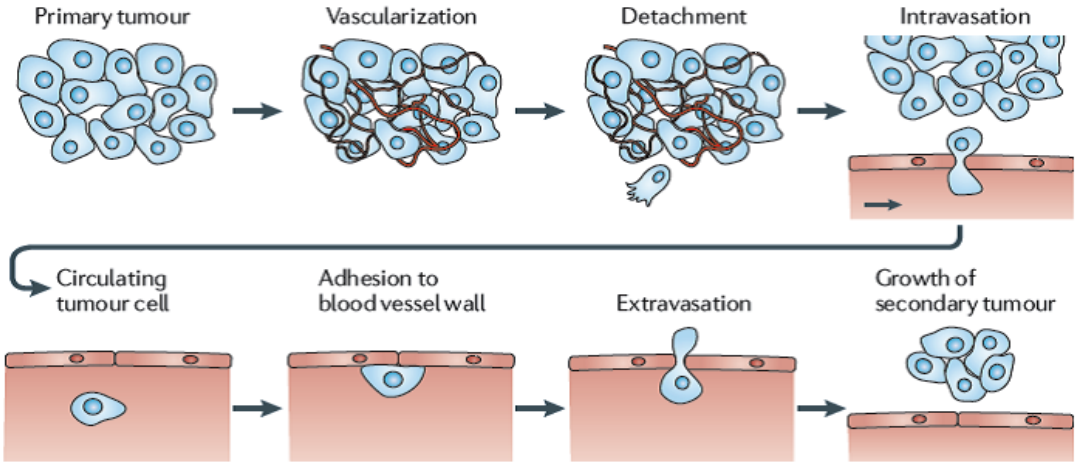

Figure 1: **Metastasis cascade.** The cartoon depicts the mechanism of metastasis and the various steps involved before a tumor cell can generate a secondary tumor. [7]

Once the tumor is vascularized, tumor cells are able to detach from the primary tumor and undergo intravasation into the blood vessel, which allows the tumor cells to circulate within the vascular system. The detachment of tumor cells from the primary site involves the epithelial to mesenchymal transition (EMT), where a reduction in E-cadherin and cytokeratins leads to significant changes in both physical and chemical properties of the cells. The adaption to a mesenchymal morphology is accompanied by the secretion of matrix metalloproteinases (MMPs), which digest and remodel the basement membrane.[8,9] After detachment, tumor cells migrate through the extracellular matrix (ECM), which is rich in collagen I. The tumor cells are able to digest the collagen-rich ECM via the secretion of MMPs, allowing them to migrate through the matrix via pseudopodial protrusions regulated by the Arp2/3 complex and focal adhesion proteins.[10]

Once tumor cells successfully undergo intravasation into the blood vessels, these circulating tumor cells can adhere to the blood vessel wall and undergo extravasation, which like the process from detachment to intravasation, requires morphological and chemical changes. If the tumor cells progress through all of these stages, a secondary tumor can grow at a distal site.

1.4 Single cell migration through a collagen I matrix

In a three-dimensional (3D) collagen I matrix, we are able to study cell migratory phenotypes and how they degrade the collagen matrix. Collagen is the most abundant fibrous protein within the interstitial ECM and supports chemotaxis and migration.[11] During single cell migration, tumor cells are exposed to the collagen rich extracellular matrix, which the cells can remodel to be stiffer and more suitable for their growth. MMPs are secreted and activated by tumor cells to further remodel the ECM and basement membrane and initiate the release of ECM-embedded growth factors.[11] The degradation and manipulation of the ECM is closely correlated with enhanced cellular migration through the matrix.

The migration of tumor cells through a collagen-rich ECM is modulated by the generation of pseudopodial protrusions, which allow tumor cells to stiffen and remodel the collagen matrix. The protrusions are regulated by focal adhesion components, which are composed of clustered integrins that connect the cellular actin network to the ECM fibers.[10] It has been demonstrated that protrusions generated in 3D environments are both multigenerational and dendritic. Protrusions that emerge directly from the cell body (referred to as mother protrusions) are specifically

regulated by FAK, talin, and p130Cas. Studies have shown that the protrusions that stem from mother protrusions (referred to as daughter protrusions) are regulated by the Arp2/3 complex as well as N-WASP, WAVE1, cortactin, Cdc42, and VASP. It is the rate of generation of these daughter protrusions, not the length, that is closely associated and can predict cell speed in 3D collagen I matrices.[10]

In this study, we utilize a 3D cell culture system that closely simulates the collagen-rich ECM of tumor tissue. This 3D system provides a comprehensive and rapid method to analyze tumor cell migration and proliferation. Cells suspended in this 3D matrix are easily visualized by phase contrast microscopy and easily treated with various reagents, which allows for extensive screening of biological responses to growth factors and chemical agents.

1.5 Motivation for the study

Current therapies for TNBC and PDAC have mechanisms of action that are anti-proliferative, yet metastasis is responsible for the vast majority of deaths in these types of cancer. Previous studies have demonstrated new insights into the mechanisms that govern metastasis by elucidating a relationship between local tumor cell density and migration. These insights have helped researchers establish new therapeutic targets that solely target metastasis through the inhibition of IL-6 and IL-8. With this basis, two projects were conducted to further explore the migratory phenotypes of these highly metastatic cancers. TNBC cells, MDA-MB-23, were studied in a much more compact high-cell density environment with a specific focus on the impact of E-cadherin on migratory phenotype shifts and invasion. Another highly metastatic cancer – pancreatic ductal adenocarcinoma – was also studied to demonstrate that the synergistic signaling between IL-6 and IL-8 could be exploited to inhibit the highly metastatic nature of PDAC.

2 Migratory phenotypes

During detachment, tumor cells adopt a migratory phenotype that allows them to move through the ECM.[12] Traditionally, cellular migration has been studied on two-dimensional, flat surfaces, which do not recapitulate the *in vivo* environment. The use of three-dimensional collagen I matrices allows us to simulate the collagen rich environment these tumor cells migrate through *in vivo*. The generation and use of a realistic model to study cellular migration has provided new insights into the dynamics of cellular migration.[10,13,14]

Many factors can impact a cell's migratory phenotype, including environmental factors and genetic factors.[13,14] We explored the impact of both environmental and genetic factors on cell migratory phenotypes in a 3D system. When tumor cells initially break away from the primary tumor during the detachment stage, they are in a high cell density environment. When the cells leave the ECM and undergo intravasation, their environment changes drastically and their migratory phenotype shifts, suggesting cell density has an impact on the migratory phenotype of cancer cells.

From a clinical data perspective, certain genes are associated with worse prognoses. For TNBC, elevated expression of E-cadherin is associated with a lower recurrence free survival rate when compared to patients with a lower expression of E-cadherin.[15] The impact of both an environmental factor (cell density) and a genetic factor (high expression of E-cadherin) has been explored to better understand how to prevent these enhanced migratory and invasive phenotypes seen in both PDAC and TNBC.

2.1 Mechanism of cell-density dependent migration in TNBC

The impact of cell density on the migratory patterns in TNBC cell line MDA-MB-231 has been explored by Jayatilaka, et al. [5] Under high cell-density conditions, MDA-MB-231 cells show migratory phenotypic shifts in speed and persistence which is a direct result of the protrusion frequency (shown in Figure S8).[5] Cell-density also impacts the amount of secreted IL-6 and IL-8, shown in Figure 2.[5]

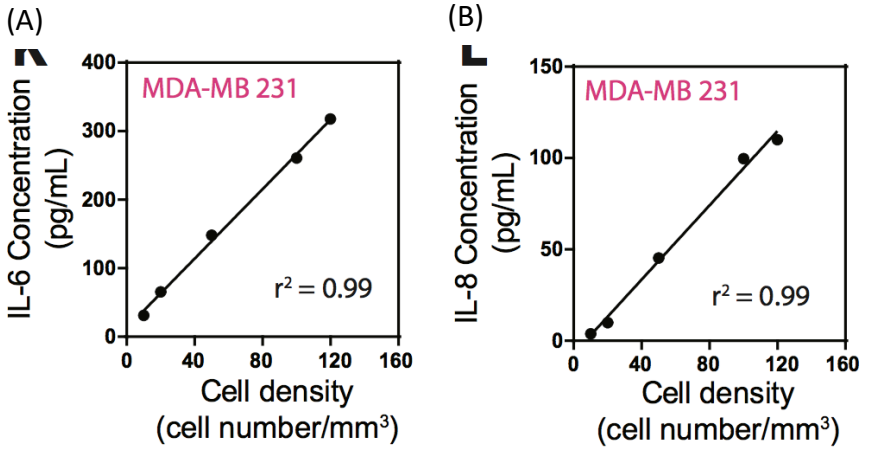

(A) and IL-8 (B) in cell supernatant was evaluated using an ELISA assay. IL-6 and IL-8 concentration in the supernatant increased with cell density. [5]

Understanding how cell density affects the migratory phenotype of metastatic cancers requires an understanding of the mechanism behind the phenotypic shift. The IL-6 and IL-8 signaling pathway leads to enhanced cell motility via the cascade depicted by Figure 3.

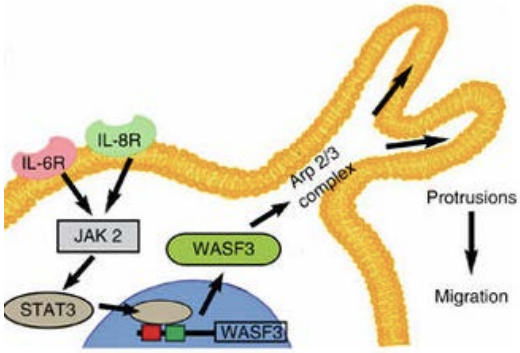

Figure 3: **Cascade initiated by IL-6 and IL-8.** The cascade initiated by the binding of IL-6 and IL-8 to their respective receptors initiates a cascade that leads to the generation of the Arp2/3 complex. [5]

Secreted IL-6 and IL-8 are sensed by their respective receptors via a paracrine pathway and initiate a cascade that leads to the enhanced generation of the Arp2/3 complex, which is directly linked to protrusions, as shown in the figure above.[5] As previously mentioned, the Arp2/3 complex, along with focal adhesion proteins, regulates pseudopodial protrusions. The rate of protrusions directly correlates with enhanced cell speed; therefore, the IL-6 and IL-8 receptors

prove to be excellent targets for therapeutic agents to decrease the generation of the Arp2/3 complex and by extension, slow the rate of protrusions and migration.[5,14]

2.2 Targeting IL-6 and IL-8 to slow metastasis

The paracrine signaling activated via IL-6 and IL-8 receptors was studied extensively by Jayatilaka, et al. [5]. The intermediate pathway shown in Figure 3 was mapped out using RNA-sequencing as well as qPCR, protein, and inhibitor studies. Inhibitors of IL-6 (Tocilizumab, Genentech), IL-8 (Reparixin, Med Chem Express), JAK2 (AG-490, Santa Cruz Biotechnology), STAT3 (S3I-201, Santa Cruz Biotechnology), and Arp2/3 complex (CK 666, Sigma Aldrich) were all used to map out the pathway depicted in Figure 3. It was determined that inhibiting IL-6 and IL-8 (with Tocilizumab and Reparixin) was most effective in slowing the migration of tumor cells in a 3D collagen I matrix.

2.2.1 Tocilizumab and reparixin – mechanism of action

Tocilizumab is the first FDA approved agent that prevents IL-6 from binding to its receptor. It is a monoclonal antibody that competitively binds to the IL-6 molecule's receptor and therefore prevents IL-6R signal transduction to inflammatory mediators that summon B and T cells.[16] Based on the results from clinical trials for the treatment of arthritis, it has been determined as a safe alternative to methotrexate (the current standard of treatment) and also safe to be used in combination with methotrexate to reduce inflammatory response. Both of these points are important to note, when considering using Tocilizumab in combination with other agents.

Reparixin is an CXCR1/2 antagonist that acts as an IL-8 receptor inhibitor and is currently in clinical trials to treat breast cancer. CXCL8 (IL-8) binds to CXC R1/2, as a crucial member of leukocyte recruitment.[17] Reparixin is a non-competitive allosteric blocker of CXCR1/2 but has higher efficacy in inhibiting CXCR1.[17] The mechanism of action for both tocilizumab and reparixin is shown in Figure 4.

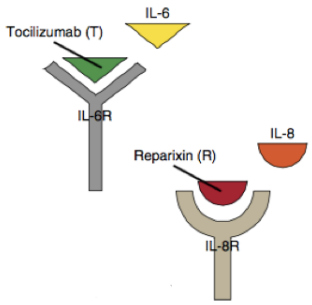

Figure 4: **Mechanism of action for tocilizumab and reparixin.** Tocilizumab and reparixin inhibit IL-6 and IL-8, respectively, by binding to the receptors.[5]

2.2.2 Impact of tocilizumab and reparixin combination therapy on metastatic burden

The combination of tocilizumab and reparixin reduced metastatic burden without affecting tumor growth in an *in vivo* study with MDA-MB-231 conducted by Jayatilaka, et al. [5] This novel combination therapy reduced metastasis to the organs most frequently affected by metastasis in breast cancer, shown in Figure 5.[5] The combination was the only treatment that reduced metastasis to the lungs, liver, and lymph nodes.

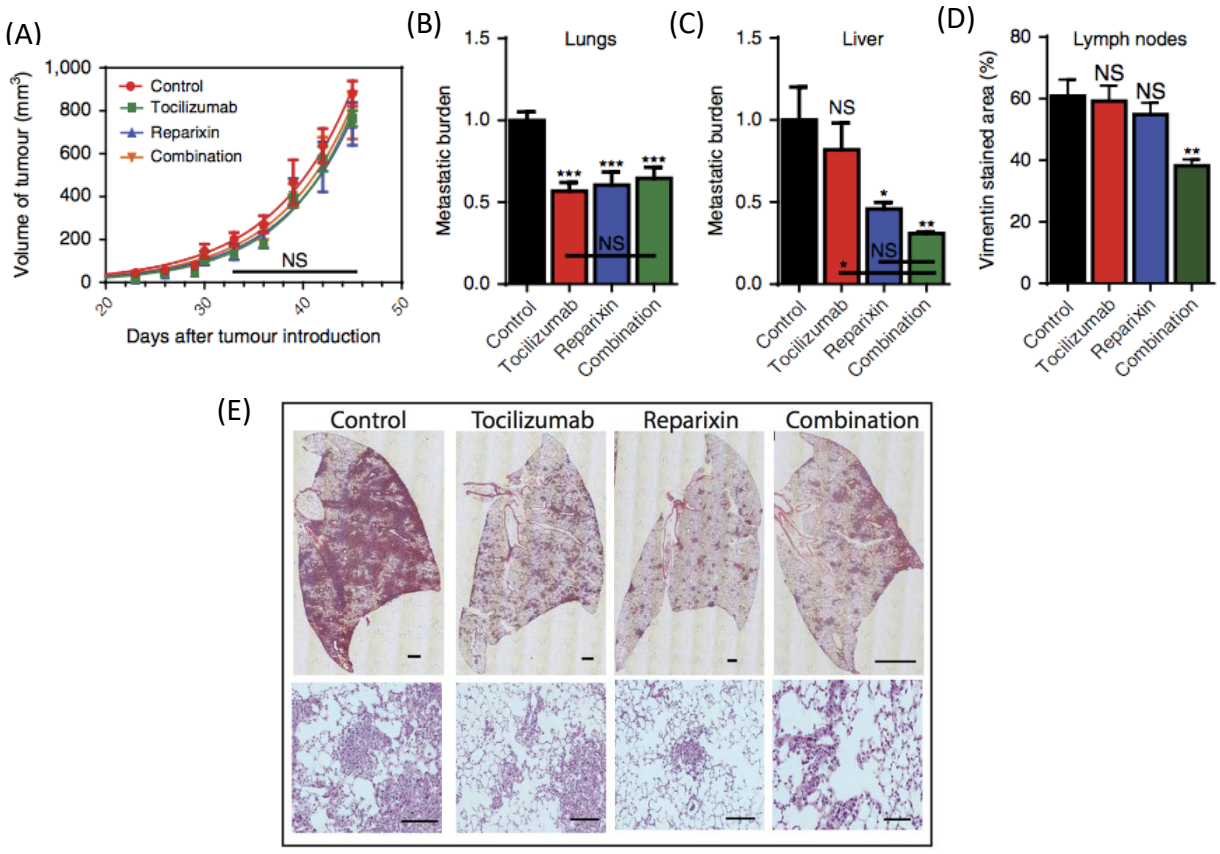

Figure 5: **Impact of tocilizumab and reparixin on tumor volume and metastatic burden.** The impact of tocilizumab and reparixin alone in comparison to their combination is shown in a-d. (A) shows that tumor volume was not impacted by treatment with tocilizumab, reparixin, or the combination therapy when compared to the control. (B), (C), and (D) show the metastatic burden to the lungs, liver, and lymph nodes is significantly decreased with a combination treatment of both tocilizumab and reparixin. Metastatic burden was measured by conducting qPCR of the H2K gene. (E) H&E staining of excised lungs further validating the metastatic burden to the lungs is decreased with the combination of T+R. [5]

The discovery of this novel pathway gives insight into the mechanism by which cancer cells metastasize from a localized tumor site, laying the groundwork for future studies of highly metastatic cancer types.

2.3 Impact of E-cadherin on migratory phenotype

2.3.1 E-cadherin: the tumor suppressor gene

E-cadherin is a cell-cell adhesion molecule that plays an important role in epithelial cell behavior, tissue formation, and some research shows it plays a role in suppressing cancer.[18] More generally, E-cadherin is part of the cadherin family, a large category of transmembrane glycoproteins that mediate specific cell-cell adhesion via Ca^{2+} dependence. There are five major subfamilies of cadherins, but E-cadherin belongs to the 'classical' or type I subfamily and is one of the most extensively studied classical cadherins.[18] E-cadherin is specifically associated with three catenins (alpha, beta, and p120) which link E-cadherin to the actin cytoskeleton.[19] An overview of the E-cadherin-catenin complex between two epithelial cells is shown in Figure 6, demonstrating how E-cadherin facilitates cell-cell adhesion with the help of intracellular catenins, among other proteins.

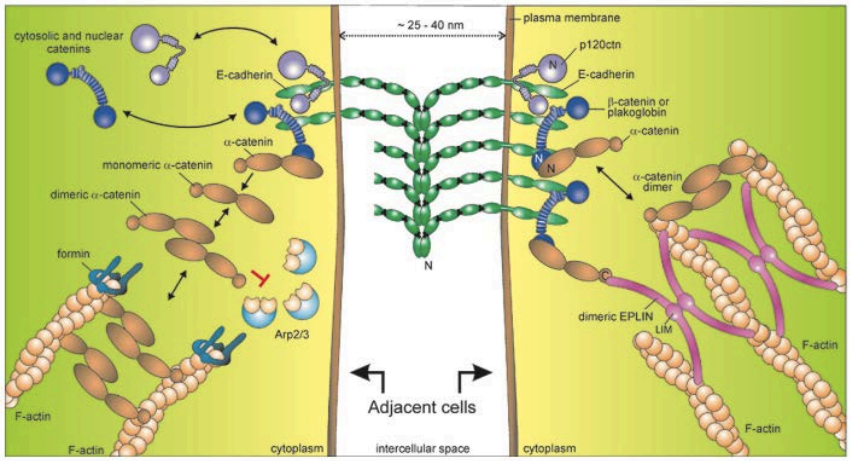

Experimental evidence has shown that the loss of E-cadherin correlates with increased

Figure 6: **Schematic overview of E-cadherin-catenin complex.** Shows the E-cadherin-catenin complex (CCC) at the junction between two neighboring epithelial cells, showing the involvement of intracellular proteins in the facilitation of cell-cell adhesion. [18]

metastasis and invasion, as it is thought that loss of E-cadherin promotes metastatic dissemination by disrupting intercellular contacts.[19] As studied by Onder, et al. [19], the loss of E-cadherin promotes the disaggregation of cancer cells because it disrupts cell-cell adhesion within in a tumor. It has also been shown that the suppression of E-cadherin function leads to mesenchymal morphology and increased cellular migration and invasion.[20]

2.3.2 Paradox of E-cadherin

Based on an *in vitro* study conducted at Harvard Medical School, CDH1, the gene that encodes E-cadherin protein, was determined to be a tumor suppressor gene (TSG), not an oncogene.[21] Figure 7 shows the genes analyzed in the study, where red boxes denote TSGs and green boxes denote oncogenes.

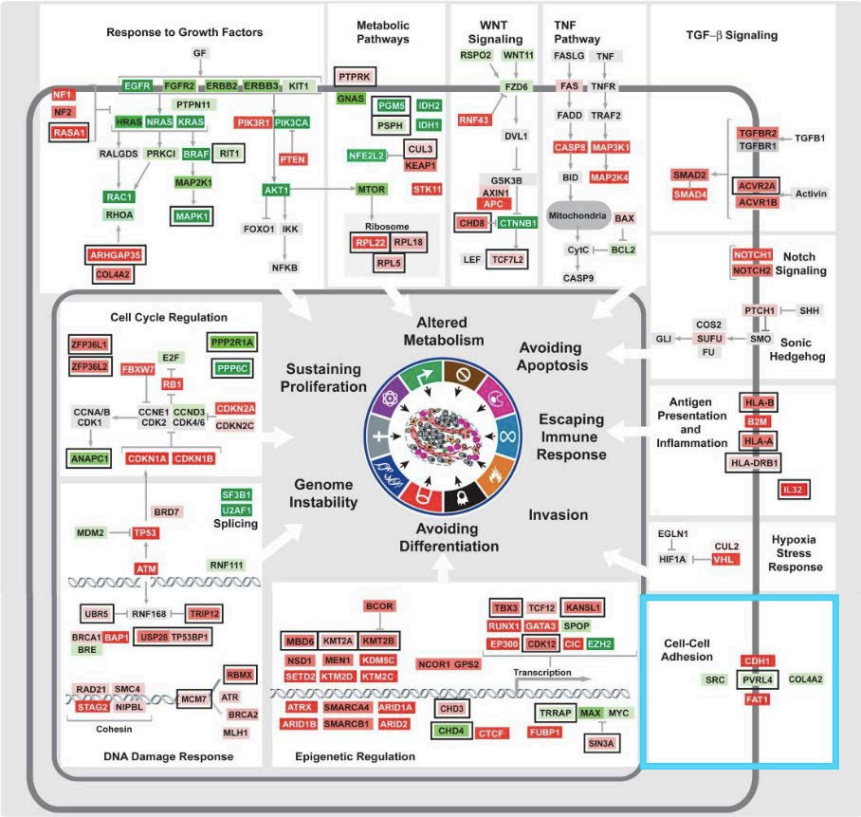

Figure 7: **Schematic of the genes analyzed**. Shows the analyzed tumor suppressor genes and oncogenes in their respective pathways and how they come together to impact cell function. The blue box highlights the cell-cell adhesion pathway, where CDH1 is shown in red, denoting it as a tumor suppressor gene. [19]

Previous studies have questioned if E-cadherin is truly a tumor suppressor gene, suggesting that previously thought TSG may actually be an oncogene, promoting a more invasive migratory phenotype.[15] We further explored the impact of E-cadherin expression in a clinical setting, shown in Figure 8.

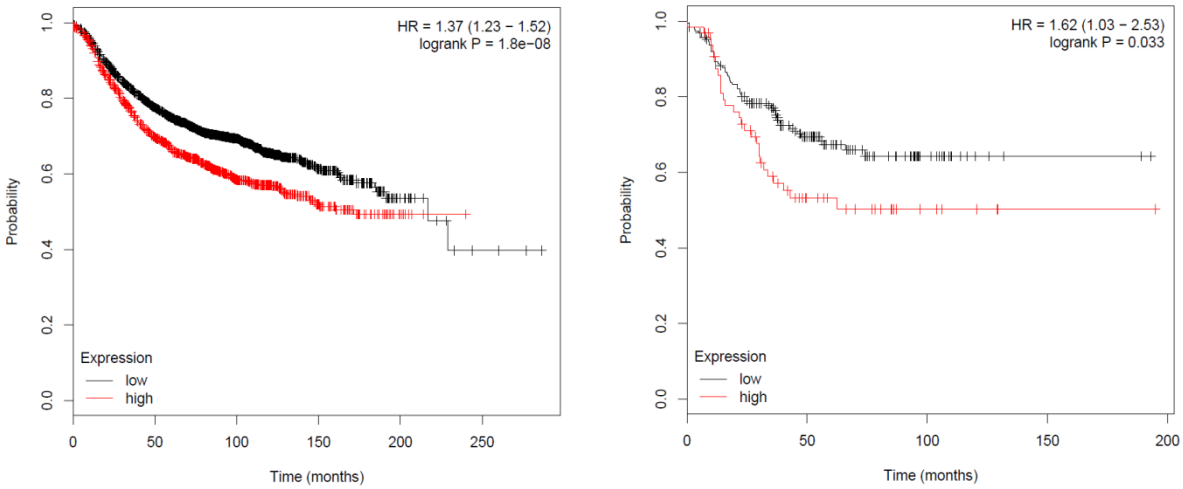

Figure 8: **Recurrence probability for patients expressing E-cadherin.** (A) shows the correlation between high expression E-cadherin (red) compared to low expression of E-cadherin (black) for all subtypes and stages of breast cancer. (B) shows the correlation between high and low expression of E-cadherin for TNBC subtype, all stages. Graphs were generated using Kaplan-Meier database.[38]

The data in Figure 8 shows patients with a high expression of E-cadherin have a significantly lower relapse free survival probability when compared to patients with low expression of E-cadherin. However, loss of E-cadherin has been shown to promote metastasis and invasion. Since there is a large disconnect between experimental data and clinical data, we further explored the role of E-cadherin in triple negative breast cancer cells.

2.3.3 Impact of E-cadherin on TNBC

The paradoxical role of E-cadherin has been previously explored, as it is still not well understood how E-cadherin over-expression results in a worse prognosis in a clinical setting. Previous studies show the impact of E-cadherin overexpression in the same triple negative breast cancer cell line studied by Jayatilaka *et al*, MDA-MB-231. Utilizing a novel, double-layered spheroid model, the *in vitro* results, shown in Figure 9, correlated with the clinical data shown in Figure 8; an overexpression of E-cadherin correlated with more invasive migratory phenotype.

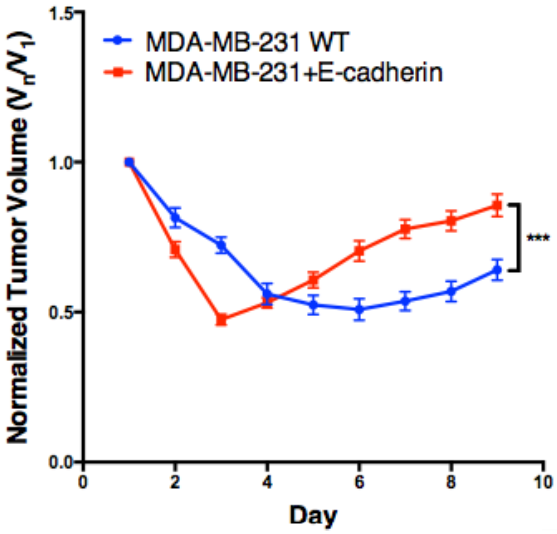

Figure 9: **Normalized spheroid volume over time.** Shows over-expression of E-cadherin correlates with faster spheroid progression when compared to lower-expressing E-cadherin spheroids. (Ong, *et al*. JHU, unpublished data).

To further test this result, we conducted an *in vivo* study to test the impact of E-cadherin overexpression in mice injected with MDA-MB-231 into the mammary fat pad of NSG mice. The results are shown in Figure 10, confirming the correlation of E-cadherin with increased tumor progression.

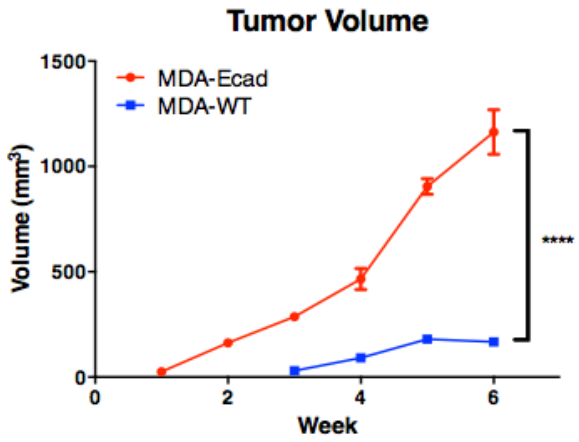

Figure 10: **Tumor volume over time for *in vivo* study.** Tumor volume was measured weekly in mice injected with MDA-MB-231 WT and MDA-MB-231 + E-cadherin. Tumors generated from cells over-expressing E-cadherin progressed much faster when compared to low-expressing E-cadherin tumors (MDA-WT). (Gilkes *et al*, JHMI, unpublished data).

Based on Figures 9 and 10, the double layered spheroid model is able to recapitulate the *in vivo* correlation of E-cadherin. The mouse study conducted was primarily to demonstrate the increased proliferation that is correlated with overexpression of E-cadherin

3 A novel spheroid model to study migratory phenotypes in TNBC

The paradox of E-cadherin needs to be further explored as research data that suggests E-cadherin is a tumor suppressor gene conflicts with clinical data that shows higher expression of E-cadherin correlates with lower recurrence free survival. To further study the impact E-cadherin has on proliferation and tumor progression, a new spheroid model was developed that strived to recapitulate the tumor microenvironment more accurately.

3.1 Double-layered spheroid model (3DLTS)

A novel, double layered spheroid system was developed to better study cancer cells *in vitro*. Current methods of spheroid generation use mechanical manipulation to form cells coated in either matrigel or collagen into a compact spherical shape.[22] However, a novel method of double-coated spheroids gives a more realistic model by including a "basement" membrane composed of matrigel and a collagen I layer to mimic the stromal layer surrounding tumors. In comparison to organoid models, this system utilizes collagen as the stroma layer surrounding the inner spheroid that is mixed with matrigel. Most organoid models utilize matrigel to simulate the ECM, not collagen.[23] However, the utilization of collagen to simulate the tumor stroma (ECM) allows for better drug penetration compared to matrigel.[24] This main difference allows for a more high-throughput drug screening application.

Previous studies have shown that cells over-expressing E-cadherin invade the collagen coating, which simulates the tumor stroma, in half the time when compared to cells not expressing E-cadherin, shown in Figure 11.

(A) 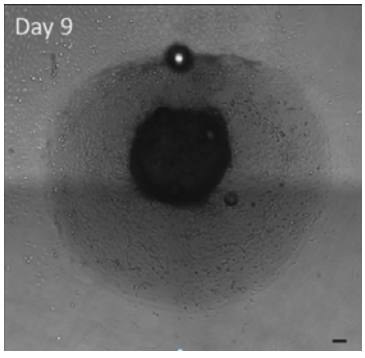

(B) 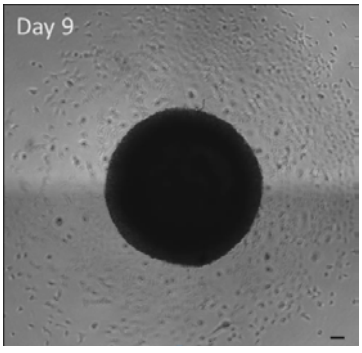

Figure 11: **Spheroid progression differences seen in over-expression of E-cadherin.** Comparison of 3DLTS progression in MDA-WT and MDA+E-cadherin at day 9, demonstrating that MDA+E-cad leads to increased tumor progression. (Ong *et al*, JHU, unpublished results).

As shown in Figure 11, the MDA-MB-231 + E-cadherin 3DLTS invaded the tumor stroma in 9 days, compared to the MDA-MB-231 WT 3DLTS, which took 19 days to completely invade the tumor stroma. This supports the *in vivo* mouse model results shown in Figure 9. With this basis, further studies were conducted to understand how the over-expression of E-cadherin was impacting the cells migratory and invasive phenotypes.

3.2 How E-cadherin affects invasive phenotype

As shown in the above sections, both *in vitro* and *in vivo* studies showed over-expression of E-cadherin correlates with faster spheroid progression, which is one of the defining characteristics of metastatic cells. We also observed that over-expression of E-cadherin induces a change in invasive phenotype of the cells as they migrate from the inner spheroid into the collagen layer. As shown in Figure 12a, MDA-MB-231 WT 3DLTS exhibit a collective cell migration from the inner spheroid into the collagen layer, where a few cells are migrating through the collagen layer together and invade further into the collagen layer. In Figure 12b, MDA-MB-231+E-cadherin 3DLTS exhibits a 'connected' cell migration into the collagen layer, invading as a unified band of cells.

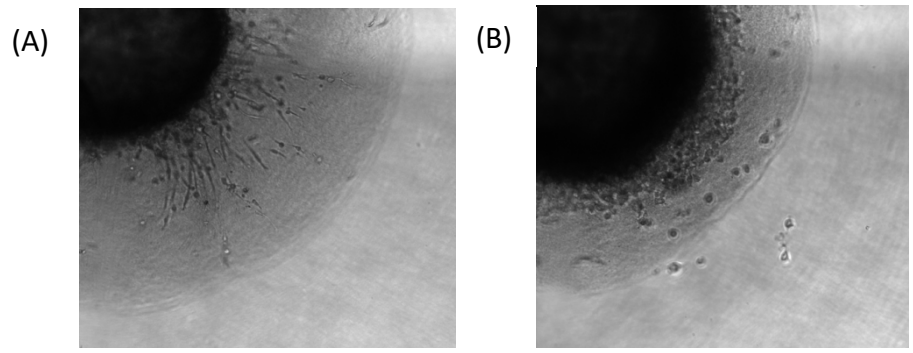

Figure 12: **Invasive phenotype induced by E-cadherin over-expression.** (A) MDA-MB-231 WT 3DLTS exhibits a collective cell invasion from the inner spheroid into the tumor stroma. (B) MDA-MB-231+E-cadherin exhibits a 'connected' cell migration from the inner spheroid into the tumor stroma. (Ong *et al*. JHU, unpublished results.)

To understand how E-cadherin impacts the behavior of TNBC cells, three different signaling pathways were studied at the mRNA level to see if overexpression of E-cadherin has any downstream impacts on gene expression. The MAPKinase, WNT, and HIPPO pathways were

selected based on previous research that links E-cadherin loss or gain of expression to having impacts on intermediate proteins within these complex pathways.

3.2.1 MAPKinase signaling pathway and the role of ERK, JNK, p38

The MAPKinase pathway (shown in Figure S2) consists of a three-tiered kinase cascade that includes a MAP kinase kinase kinase (MAP3K or MEKK), a MAP kinase kinase (MAP2K or MEK), and a MAP kinase (MAPK).[25] In our studies, we focused on the genes that encode the MEK and MAPK protein complexes as well as downstream proteins from those cascades. ERK is the most well-studied pathway within MAPKinase singaling.[25] Activated Raf (b-Raf is the strongest MEK kinase) activates MEK1 and MEK2 by phosphorylating serines 218 and 222, which then activate ERK1/2 via phosphorylation of tyrosine 204 and 187, respectively. Once activated, ERK can phosphorylate numerous cytoplasmic and nuclear targets, which in turn leads to ERK having the ability to regulate processes such as proliferation, differentiation, survival, migration, angiogenesis, and chromatin remodeling.[25]

The JNK pathway is considered a stress activated pathway within MAPKinase signaling. Activation of JNK requires the dual phosphorylation of tyrosine and threonine residues at a distinctive TPY motif, which is catalyzed by MEK4 and MEK7.[25] JNK also has the ability to translocate from the cytoplasm to the nucleus and phosphorylate a number of transcription factors, including AFT-2 and STAT-3. In response to stresses, JNK interacts with p53, a well-studied mutation in many cancer types.

The p38 pathway is also considered a stress activated pathway within MAPKinase signaling and can also translocate from cytoplasm to the nucleus. p38 is activated by environmental stresses and inflammatory cytokines. Activated p38 is involved in the regulation of apoptosis, cell cycle progression, growth, and differentiation.[25]

3.2.2 WNT signaling pathway and the role of beta-catenin

Early studies of WNT suggest that it can be linked to the malignant transformation of mouse mammary tissue. Recent studies have demonstrated WNT signaling is a central mechanism in cancer cell biology.[26] We chose to study the genes that encode the proteins involved in the main scaffold of the WNT canonical pathway (shown in Figure S3) because it causes an accumulation of beta-catenin, which is known to exclusively form a complex with E-cadherin. Beta-catenin is negatively regulated by AXIN-1 and APC. In order to understand the impact over-expression of

E-cadherin has on the WNT pathway, we focused on the proteins surrounding beta-catenin as well as downstream complexes that regulate the cell cycle.

3.2.3 HIPPO signaling pathway and the role of YAP/TAZ

The HIPPO pathway (shown in Figure S3) controls organ size and tissue growth during development, regeneration, and cancer.[27] TAZ and YAP are two key components of the HIPPO signaling pathway and have been studied in depth for their role in cancer-related HIPPO signaling. Genetic variations in the HIPPO pathway in TNBC have been linked to over-expression of TAZ (J Zhang). TAZ and YAP hyper-activation leads to abnormal cell proliferation, a hallmark of cancer and metastasis.[4,7,27] It has been shown that overexpression of TAZ/YAP can promote cell survival both *in vivo* and *in vitro*. In cancer cell lines, the overexpression of TAZ/YAP results in resistance to apoptosis. The WNT signaling pathway is known to functionally interact with the HIPPO pathway in many ways, but more specifically for our purposes, TAZ has been shown to interact with WNT signaling by interacting with Dvl1 in the cytoplasm and YAP or TAZ can interact with beta-catenin and keep it in the cytoplasm.[27,28] With these interactions in mind, we chose to study parts of the HIPPO pathway that lead to the transcription of genes that result in pro-proliferation as well as the interactions with beta-catenin in the WNT signaling pathway.

3.3 RT-PCR to evaluate signaling pathways

To evaluate the selected pathways, quantitative real time PCR was used to evaluate the relative gene expression of selected genes in MDA-MB-231 WT and MDA-MB-231 + E-cadherin, modeled in the 3DLTS system.

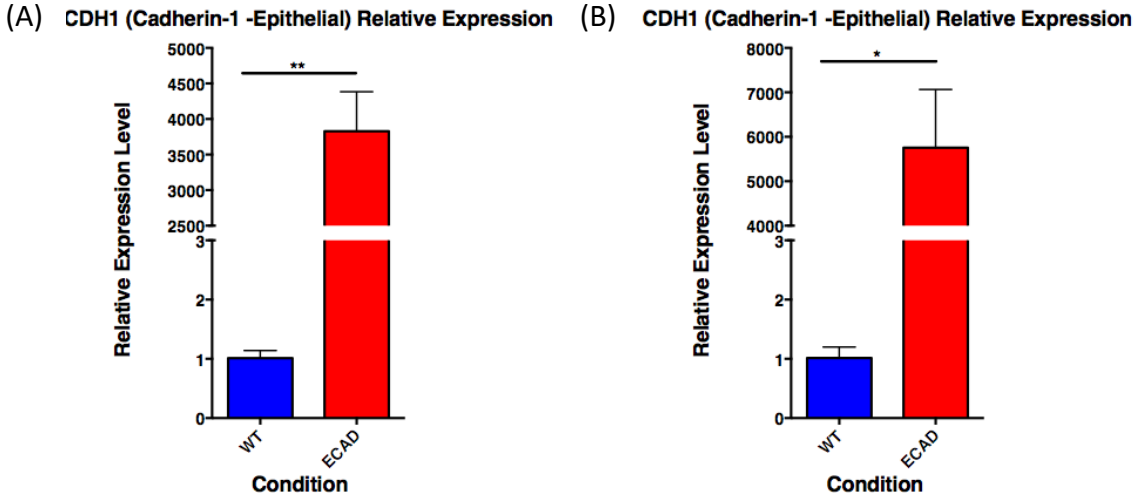

Figure 13: **Relative expression of CDH1 in 2D and 3D conditions.** Shows the relative expression of CDH1, the gene that encodes E-cadherin in MDA-MB-231+E-cadherin (red) compared to MDA-MB-231 WT (blue) in both 2D condition (A) and 3DLTS (B). (N = 3)

In Figure 13, the relative gene expression for CDH1, the gene that encodes E-cadherin protein, is shown to be significantly upregulated in MDA-MB-231 + E-cadherin when compared to MDA-MB-231 WT. This confirmation shows successful transduction of E-cadherin into the cell line and preservation of E-cadherin over-expression in 3DLTS system.

3.3.1 PCR Results- MAPKinase signaling pathway

The relative gene expression for the MAPKinase signaling pathway is shown below in Figure 14 (A-C). Our results show that there is significant upregulation of FOS, MAP2K1, MAPK1, MAPK14, MAPK3, MAPK8, and MAPK9. These genes encode proteins involved in the ERK, JNK, and p38 cascades within the MAPKinase signaling pathway.

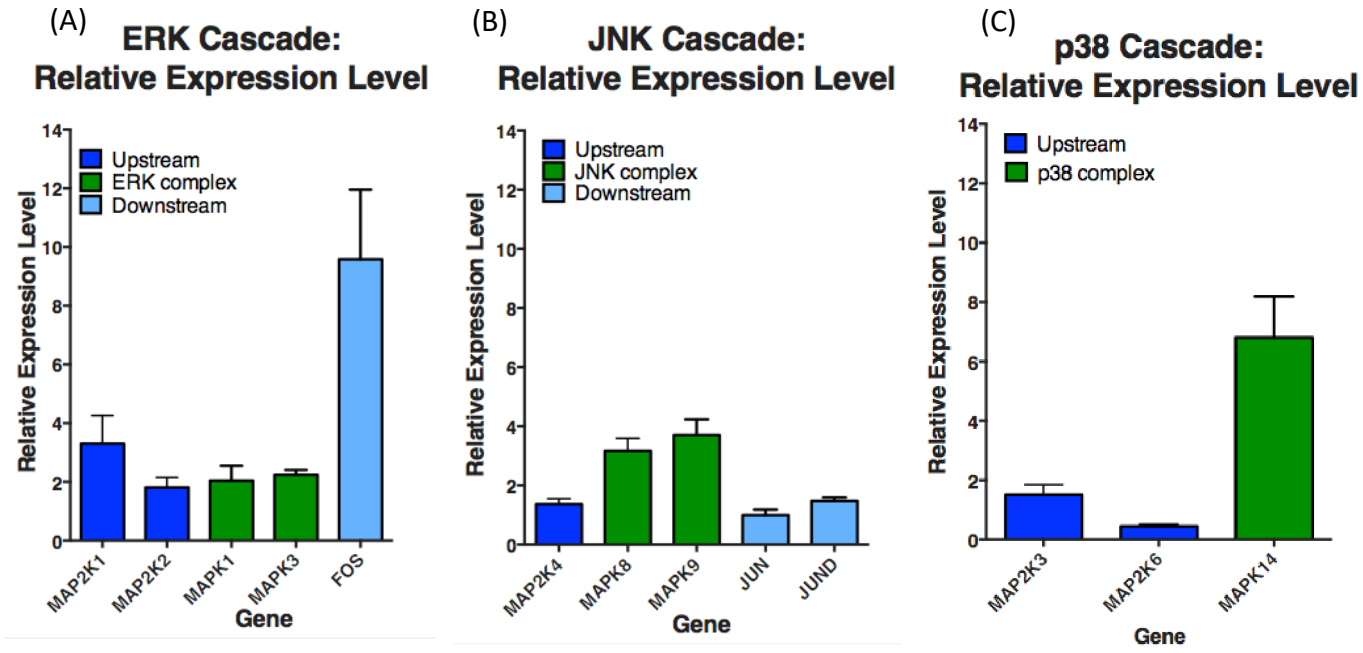

Figure 14: **Relative Gene Expression of MAPKinase Signaling.** Relative gene expression of MDA-MB-231 +E-cadherin compared to MDA-MB-231 WT. Upregulation is considered above a 2-fold increase. (A) shows upregulation of the ERK cascade, (B) shows upregulation of the JNK complex, and (C) shows upregulation of the p38 complex. (N = 4)

The ERK cascade was significantly upregulated both upstream and downstream from the ERK1/2 complex, suggesting that the impact of E-cadherin on the MAPKinase pathway can be reversed with the inhibition of ERK1/2.

3.3.2 PCR Results- WNT signaling pathway

The relative gene expression for the WNT signaling pathway is shown in Figure 15. Our results show there is a significant upregulation of APC, CCND1, CSNK1A1, CSNK2A1, CTNNB1, GSK3Beta, HDAC1, LEF1.

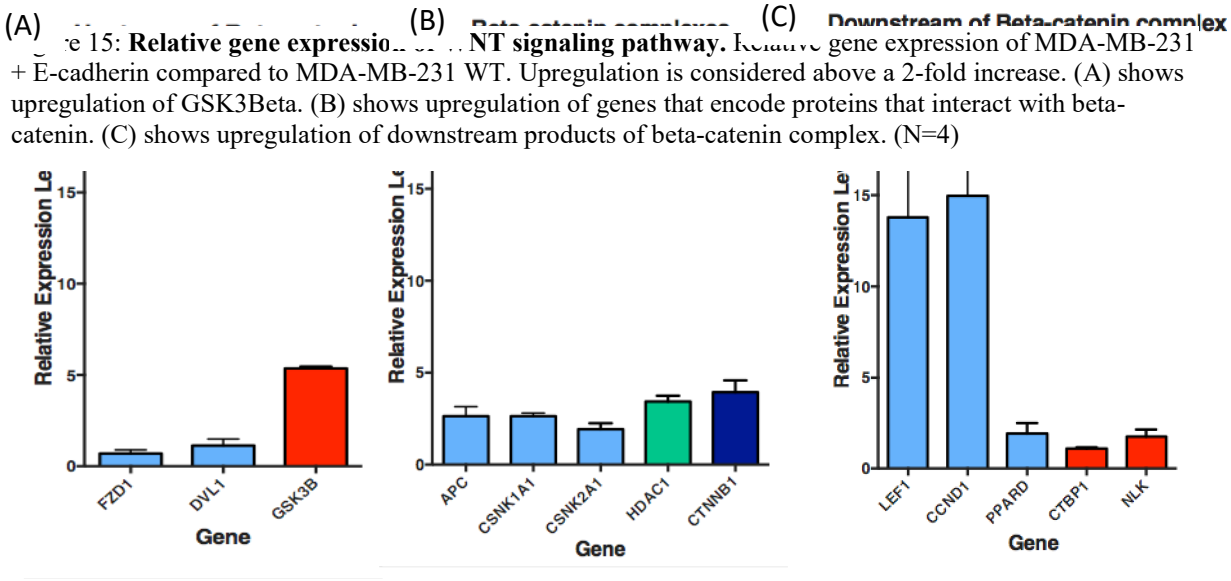

e 15: **Relative gene expressio.. ..NT signaling pathway.** Relative gene expression of MDA-MB-231 + E-cadherin compared to MDA-MB-231 WT. Upregulation is considered above a 2-fold increase. (A) shows upregulation of GSK3Beta. (B) shows upregulation of genes that encode proteins that interact with beta-catenin. (C) shows upregulation of downstream products of beta-catenin complex. (N=4)

As expected, we observed a significant upregulation of beta-catenin in MDA-MB-231+E-cadherin, but we also saw upregulation of many genes that encode proteins surrounding the beta-catenin protein complex as well as genes that encode proteins downstream of beta-catenin. The upregulation of HDAC1 is an important observation, as the upregulation of this gene that encodes the enzyme HDAC1, closely interacts with beta-catenin to regulate LEF-1 transition from a transcriptional repressor to an activator of downstream genes.[31]

3.3.3 PCR Results- HIPPO signaling pathway

The relative gene expression for the HIPPO signaling pathway is shown in Figure 16. Our results show significant upregulation of LATS1, SERPINE1, and TEAD1. As mentioned previously, the key genes for assessing the involvement of HIPPO signaling are YAP/TAZ, which we observed to be unchanged in MDA-MB-231+E-cadherin.

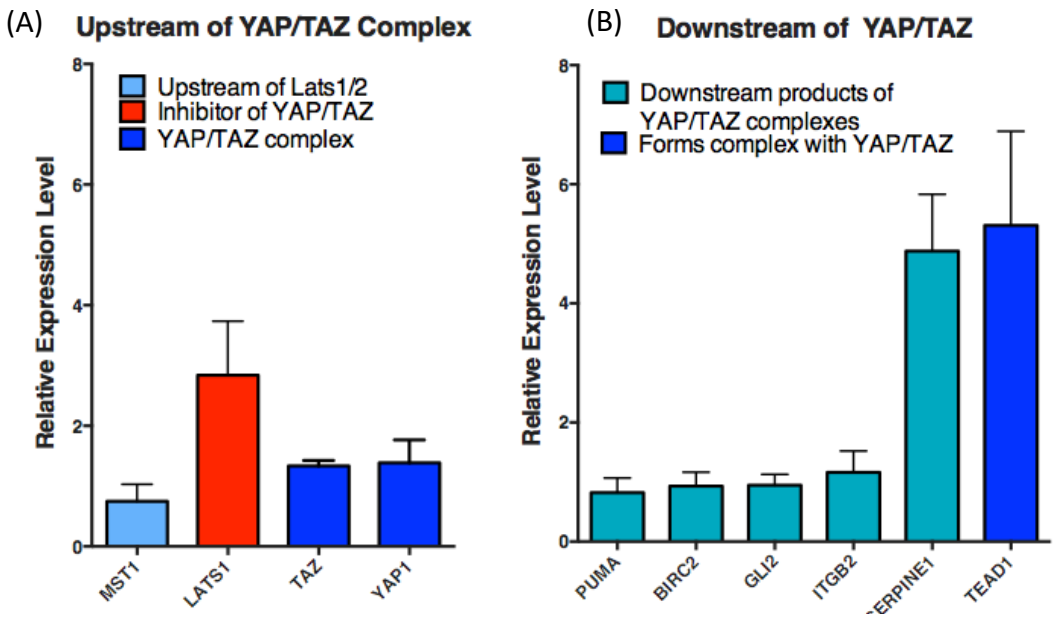

Figure 16: **Relative gene expression of HIPPO signaling pathway.** Relative gene expression of MDA-MB-231 + E-cadherin compared to MDA-MB-231 WT. Upregulation is considered above a 2-fold increase. (A) shows upregulation of an inhibitor of YAP/TAZ complex -LATS1. (B) shows upregulation a downstream product and of a protein that forms a complex with YAP/TAZ. (N=4)

The upregulation of LATS1 results in downstream impacts, such as the upregulation of TEAD1 and SERPINE1, which encodes Pai-1, a pro-proliferative protein. The unchanged expression of YAP/TAZ suggest the HIPPO signaling pathway is not significantly impacted by the overexpression of E-cadherin, since YAP/TAZ have the most widespread impact on downstream products of the HIPPO signaling pathway, shown in Figure S3. These results were used to design the drug inhibitor studies that provided insight into which gene/protein can be targeted for phenotype reversal.

3.4 Exploring ERK at the protein level

To further study the MAPKinase pathway, western blot studies were conducted to observe if there was a significant difference in the phosphorylation of ERK1/2 in MDA-MB-231+E-cadherin when compared to MDA-MB-231 WT. Since mRNA expression level of genes that encode proteins does not always translate to the protein expression, we conducted a western blot to confirm that the upregulation we observed in the gene expression of the ERK cascade is indeed present at the protein level. Shown in Figure 17, MDA-MB-231+E-cadherin has a significantly higher level of phosphorylated and total ERK1/2 when compared to WT.

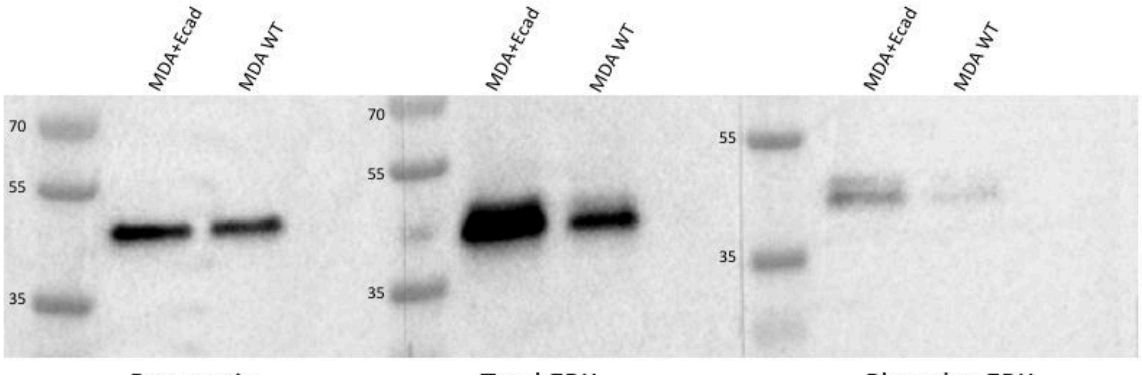

Figure 17: **Protein Expression of ERK and Phosphorylated-ERK are higher in MDA-MB-231 + E-cadherin 3DLTS.** Western blot images (A) and intensity graphs (B) of MDA-MB-231+E-cadherin compared to MDA-MB-231 WT. This confirms that over-expression of E-cadherin leads upregulation of genes in the ERK cascade translates over to the protein expression level. (N=2, but only one western blot is shown here)

Based on the Figure 17, there is a significantly higher amount of total ERK in MDA-MB-231+E-cadherin than present in MDA-MB-231 WT. This demonstrates that the mRNA levels of the genes that encode ERK1/2 correlate with the observed protein levels in the 3DLTS system.

3.5Drug inhibitor studies using 3DLTS

The development of the 3DLTS model has allowed for high-throughput drug screening experiments that can test numerous inhibitors, at numerous concentrations in a side-by-side experiment. This experimental design was implemented to study the effect of inhibitors on tumor growth rate and migratory phenotypes in both MDA-MB-231 WT and MDA-MB-213+E-cadherin.

3.5.1 Drug screening with MAPKinase and WNT inhibitors

Inhibitors for several target genes in the MAPKinase and WNT signaling pathways were selected to target various genes selected for characterization of the three pathways. In Table 1, the inhibitors selected are listed with their target genes.

Table 1: Inhibitors used for drug screening.

Inhibitor (given code)	Target (Pathway)
SP600125 (MI1)	JNK (MAPKinase)
BI-78D3 (MI2)	JNK (MAPKinase)
PD0325901(MI4)	MEK (MAPKinase)
SB203580 (MI5)	p38(MAPKinase)

Vemurafenib (MI6)	B-Raf (MAPKinase)
MK-2206 (MI7)	AKT (MAPKinase)
IWR-1-endo (WI1)	Axin2-Beta-catenin interaction (WNT)
LY317615 (WI2)	PKC (WNT)
CHIR-98014 (WI3)	GSK3beta (WNT)

A preliminary screening was done with all inhibitors and compared to MDA-MB-231+E-cadherin control to select the inhibitors to be studied more extensively. In Figure 18, MDA-MB-231+E-cadherin 3DLTS were treated with 10 μM for the screening. Only the inhibitors that showed to revert MDA-MB-231+E-cadherin back to the MDA-MB-231 WT migratory phenotype were studied more extensively.

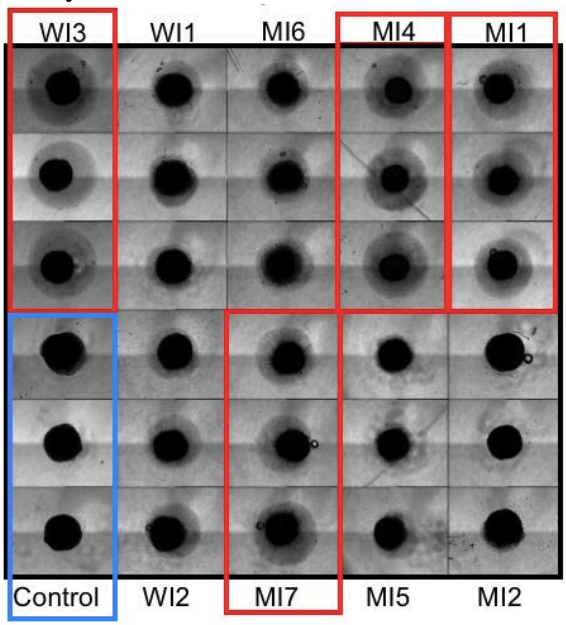

Figure 18: **Visualization of inhibitor impact on 3DLTS (MDA-MB-231 + E-cadherin).** Figure above shows the impact of each inhibitor at a concentration of 10uM (listed in Table 1) on the 3DLTS. Red boxes indicate the inhibitors that were able to preserve tumor stroma volume and prevent inner spheroid volume from progressing as quickly. Blue box is an untreated control for comparison purposes.

The data in Figure 18 was then quantified to better understand the impact the inhibitors had on the inner spheroid progression and outer stroma volume preservation. Both outer and inner tumor volume was then calculated for each inhibitor screened using a method of analysis previously outlined by Ong *et al* (Figure S1).

Figure volume (A) **ıM inhibitor screening with MDA-MB-231+E-cadh** rements from day 7 compared to day 1. (B) shows out (B) **LTS. (**A) shows ratio of the inner spheroid oid volume measurements from day 7 compared to day 1. Blue bars indicate statistical significance with a $p<0.05$. Inhibitors were selected for further screening if these volume ratios measured 1±0.5 (N=4)

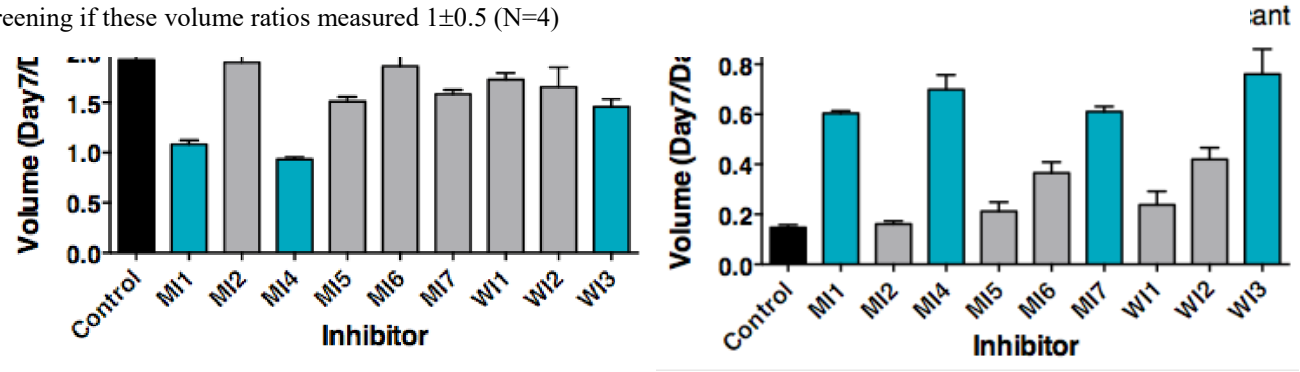

Based on the data shown in Figure 19, MI1, MI4, and WI3 inhibitors were selected for further screening. The chosen concentration of 10uM is extremely high, so another screening was done with MI1, MI4, and WI3 at 1uM concentration. The results in Figure S2 show that only MI4 was effective at a lower concentration at both preventing the inner tumor volume from progressing as quickly and preserving the stroma volume from decreasing as quickly.

This data was then compared to the mRNA relative gene expression data presented in the previous section. MI4, an MEK inhibitor, proved to be the most effective inhibitor in both preventing inner tumor volume growth and maintaining the volume of the collagen layer (stroma). Further studies were conducted to determine the optimal concentration of MI4 to revert the migratory phenotype induced by E-cadherin back to the WT migratory phenotype.

3.5.2 MEK inhibitor impact on invasive phenotype

MI4, an MEK inhibitor, proved to be the most effective at suppressing the impact of E-cadherin overexpression on the migratory phenotype. MI4 (PD0325901) has been shown to significantly reduce the growth of papillary thyroid carcinoma cells both *in vitro* and *in vivo* and is considered a second generation MEK1/2 inhibitor that prevents the phosphorylation of ERK1/2 by inhibiting MEK activation.[29] PD0325901 was previously tested for efficacy in treating melanoma and solid tumors, but the clinical trial was terminated due to severe side effects. PD0325901 is currently in the beginning stages of clinical trial recruitment for colorectal cancer and is in two active clinical trials for KRAS mutant non-small cell lung cancer and neurofibromatosis type 1.[30]

In Figure 20, the IC_{50} of MI4 is displayed as a log scale of the various drug concentrations tested. The results were used to determine the optimal concentration of the inhibitor for both inner and outer volume optimal effect.

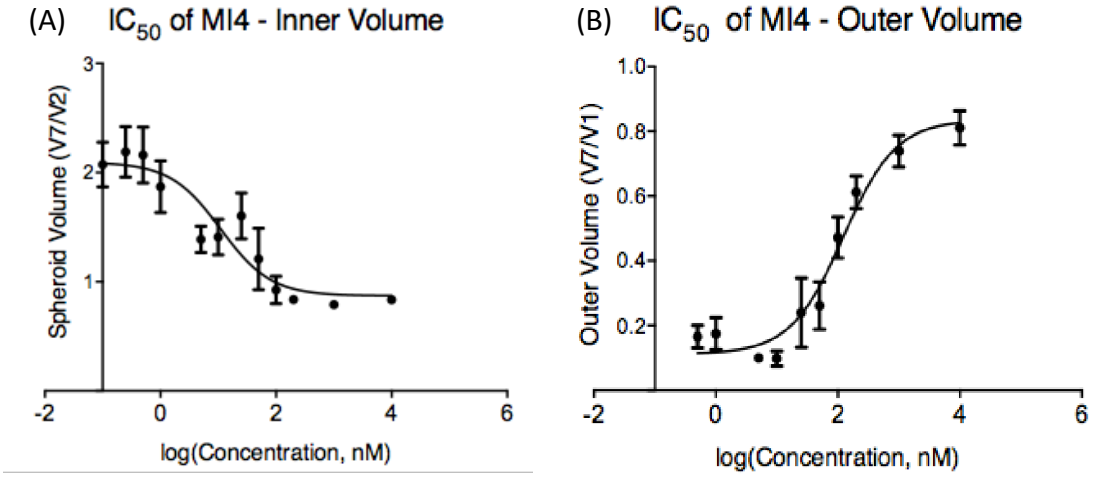

Figure 20: **IC_{50} graphs of MI4 for both the inner spheroid volume.** (A) and the outer stroma volume (B), volumes are a ratio of day 7 measurements to day 2 measurements. Results indicate the log IC_{50} of the inhibitor on the inner volume is 1.041 and for the outer volume, it is 2.088. Both of these values were used to determine optimal concentration of inhibitor for treatment of MDA-MB-231+E-cadherin 3DLTS.

As shown earlier in Figure 12, over-expression of E-cadherin also alters the invasive phenotype of the cells as they invade the tumor stroma (collagen layer). In Figure 21, the impact MEK inhibitor (MI4) has on the invasive type of 3DLTS MDA-MB-231+E-cadherin.

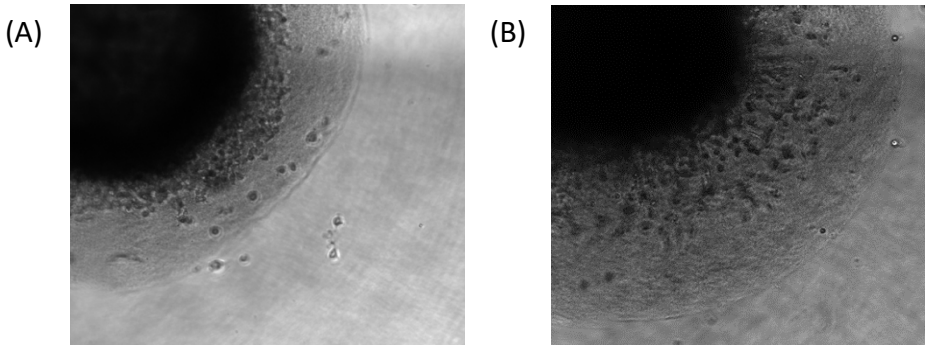

Figure 21: **Reversion of invasive phenotype with MEK inhibitor treatment.** (A) shows an untreated MDA-MB-231+E-cadherin 3DLTS control for comparison to (B) MDA-MB-231 + E-cadherin 3DLTS treated with MEK inhibitor. Images are zoomed into highlight the invasion of the cells from the inner spheroid into the tumor stroma.

MEK inhibitor (PD0325091) not only slowed the enhanced growth of MDA-MB-231+E-cadherin 3DLTS, but also reverted the invasive phenotype back to that of the MDA-MB-231 WT 3DLTS. This finding shows that the inhibition of MEK not only is effective at slowing the higher proliferation rate of MDA-MB-231+E-cadherin but also is effective at preventing the more

invasive and collective migration that is shown in Figure 21a. The mRNA gene expression analysis shows a significant upregulation of the genes that encode MEK1/2- MAP2K1/2 (expression levels shown in Figure 14a. However, an overexpression of a gene does not necessarily mean more protein is being encoded so western blot studies were conducted to confirm the increased phosphorylation of ERK1/2 (encoded by MAPK1/3) by MEK1/2 (encoded by MAP2K1/2).

3.6 Future directions

Based on these findings, more studies need to be conducted to demonstrate that MI4 (PD0325091) successfully decreases the phosphorylation of ERK1/2 in E-cadherin over-expressing cells. This will give the final confirmation that the upregulation of MEK1/2 phosphorylation of ERK1/2 in MDA-MB-231+E-cadherin is the cause for the migratory phenotype shift and higher proliferation rate seen in the 3DLTS model of these cell line subtypes. Both gene expression and proteins analyses will be conducted on treated MDA-MB-231+E-cadherin to confirm the inhibition of MEK1/2 by MI4 results in decreased phosphorylation of ERK1/2.

4 Pancreatic ductal adenocarcinoma and IL-6/IL-8 signaling

4.1 Background

Pancreatic ductal adenocarcinoma (PDAC) has a five-year survival rate of 8% for all stages combined, but for the distant metastasis stage, which accounts for 52% of patients at the time of diagnosis, the five-year survival rate is 3%.[2] Unfortunately, there has been little improvement in the past decade to improve these statistics, likely because the standard of care therapies for PDAC are anti-proliferative and do not target metastasis.[4] It is difficult to diagnose PDAC at early stages because the symptoms are generalized to abdominal pain and weight loss, which could result from any number of diseases. Unfortunately, cancer is usually one of the last considerations with such generalized symptoms so many other tests are conducted first to rule out other, less serious diseases.

4.2 Standard of care therapies

Gemcitabine is the first-line therapy offered to patients with good performance status, as it has been shown to be almost five times more effective in achieving a clinical benefit response when compared to 5-fluorouracil.[6] The primary mechanism of action for Gemcitabine is to inhibit DNA synthesis by preventing chain elongation.[31] When taken up by cells, gemcitabine is phosphorylated three times in the cell cytoplasm, resulting in the formation of gemcitabine triphosphate (dFdCTP). As shown in Figure 22, dFdCTP is incorporated into the DNA chain followed by a single deoxynucleotide. The dFdCTP initiates masked chain termination which prevents DNA polymerases from completing.

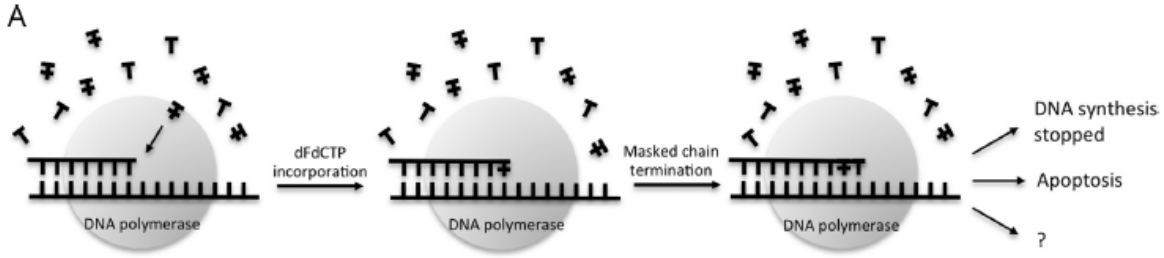

Figure 22: **Gemcitabine - Primary mechanism of action.** The replacement of one of the deoxynucleotides with dFdCTP prevents DNA synthesis by interrupting DNA polymerase formation. [31]

The secondary mechanism of action is to inhibit the enzymes associated with deoxynucleotides. Shown in Figure 23, dFdCTP directly inhibits the enzymes, whereas dFdCDP indirectly inhibits the enzymes by covalently binding to the active sites which prevents ribonucleotide reductase activation.[31] This inhibition decreases dCTP activity and increases dFdC phosphorylation.

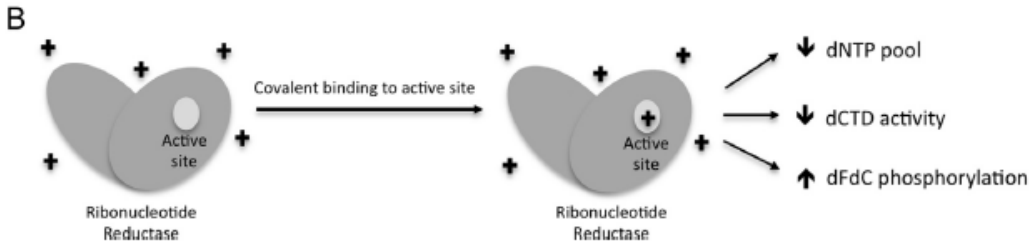

Figure 23: **Gemcitabine- secondary mechanism of action.** The dFdCDP molecules covalently bond to the active sites of ribonucleotide reductase, inhibiting activation of the molecule.[31]

Gemcitabine also activates p38 mitogen-activated protein kinase (MAPK) and induces cellular stress in tumor cells only.[31] Cellular stress leads to apoptosis in the tumor cells, but normal cells are generally not affected by this mechanism of action.

5-Fluorouracil (5-FU) is the second-line of therapies offered to patients before combination therapies will be suggested, as these combination therapies with drugs such as Abraxane and FOLFIRINOX (a combination of irinotecan, oxaliplatin, fluorouracil, and leucovorin), are highly toxic and positive response to these therapies often results in the occurrence of adverse side effects.[6] 5-FU is an antimetabolite drug that inhibits thymidylate synthase (TS) and disrupts RNA synthesis. It is an analogue of uracil, so it is able to rapidly enter the cell using the same facilitated transport mechanism as uracil.[32] 5-FU is converted into its active metabolites as shown in Figure 24: fluorodeoxyuridine-monophosphate (FdUMP), fluorodeoxyuridine triphosphate (FdUTP), and fluorouridine triphosphate (FUTP). The rate limiting enzyme in the conversion of 5-FU to its active metabolites is dihydropyrimidine dehydrogenase (DPD), which is found abundantly in the liver.[32]

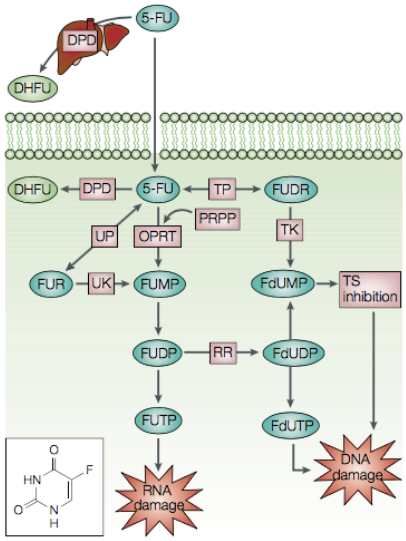

The Figure 24: **5-Fluoruoracil- Mechanism of action.** Metabolism of 5-FU resulting in DNA and RNA damage. Chemical structure of 5-FU is shown in the lower left corner.[32]

metabolite FUTP is incorporated into RNA and disrupts normal RNA processing and function. The incorporation of FUTP into RNA can result in toxicity at multiple levels, including the processing of pre-rRNA to mature rRNA, the post-transcriptional modificaition of tRNAs, and both the completion and activation of snRNA-protein complexes.[32] The metabolite FdUMP binds to the nucleotide-binding site of TS, which forms a stable ternary complex and blocks the binding

of the normal substrate deoxyuridine monophosphate (dUMP) to TS. By blocking the binding of dUMP to its binding site on TS, FdUMP effectively inhibits dTMP synthesis, shown in Figure 25. TS is an important enzyme that produces the only *de novo* source of thymidylate, which is necessary for DNA replication and repair. TS catalyzes the reductive methylation of dUMP to deoxythymidine monophosphate (dTMP), which is the reaction that produces thymidylate.[32]

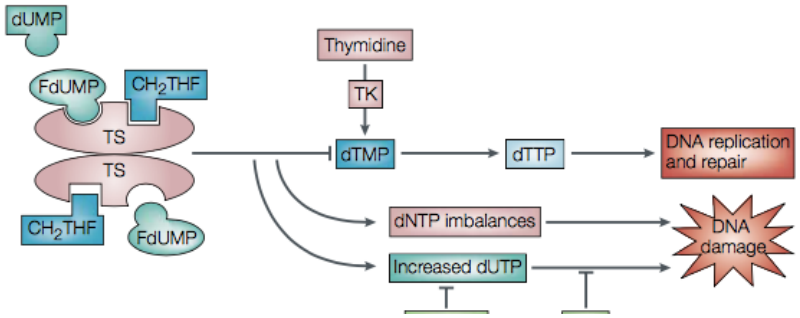

Figure 25: **5-FU-mechanism of action.** The inhibition of TS activity results in DNA damage by preventing the production of the only *de novo* source of thymidylate for DNA replication and repair.[32]

Both standard of care therapies initiate DNA damage in the cells via different mechanisms of action; however, the toxicity of these two therapies limits the possibilities of combination therapies with other chemotherapy drugs. The combinations that have been attempted so far have resulted in either higher toxicity levels in patients or significant increase in other adverse side effects of the drugs.[32] A different approach is needed to improve efficacy of treatment without increasing toxicity.

4.3 Impact of cell-density on secreted IL-6/IL-8 in PDAC

To further test the impact of IL-6 and IL-8 signaling in PDAC, we conducted a secretomic analysis using an ELISA assay. A cell line derived from a pancreatic liver metastasis, Capan-1, was used for the experiment. Cells were embedded into 3D collagen I gels at varying densities and incubated for 24 hours with fresh media. The cell supernatant was harvested and used to conduct the ELISA assays to quantify the amount of secreted IL-6 and IL-8. In Figure 26, the concentration of IL-6 and IL-8 increases with cell-density for Capan-1.

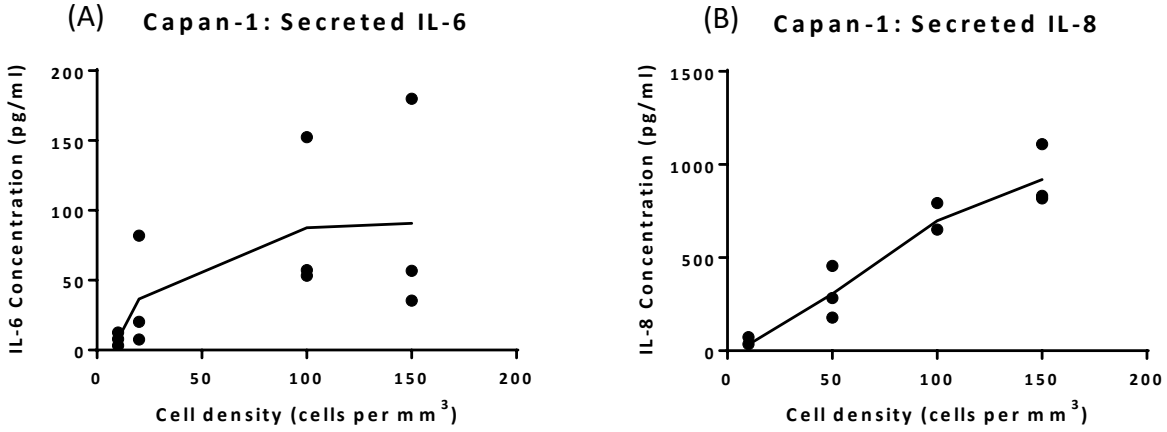

Figure 26: **Concentration of secreted IL-6 and IL-8 increase with cell density in Capan-1.** (A) ELISA assay results for IL-6 show secreted IL-6 concentration increases with cell density (N=3). (B) ELISA assay results for IL-8 shows secreted IL-8 concentration increases with cell density (N=3).

With these results, we hypothesized that the same phenomenon observed in MDA-MB-231 TNBC cells is also applicable in PDAC cells. With this basis, we designed an *in vivo* study using a PDX mouse model and proposed a combination therapy to improve efficacy of treatment for PDAC.

4.4 *In vivo* study – patient derived xenograft (PDX) mouse model

Based on the *in vitro* data, we suspected that we could prevent metastasis by inhibiting IL-6 and IL-8 with the tocilizumab and reparixin combination. Since previous combination therapies failed due to high toxicity and increased adverse side effects, we hypothesized that the combination of gemcitabine with the anti-metastatic combination would be an effective and safer way to treat PDAC. Using a subcutaneous PDX mouse model, we tested the efficacy of our proposed triple combination therapy of tocilizumab, reparixin, and gemcitabine.

4.4.1 Experimental design of *in vivo* study

In designing this *in vivo* study, we wanted to compare the final effect of just the anti-metastasis drugs (T+R), gemcitabine alone (G), and the triple combination (T+R+G) on both tumor growth and metastasis. The ½ T+R+G dose was included in the study to see if the triple combination would be effective enough to allow for a lower dose of each component and thus reduced risk. The study was broken into 5 total groups outlined in Table 2. Each condition group contained 5 mice with the exception in the ½ T+R+G group, which had 4 mice.

Table 2: PDX mouse model treatment groups and dosages for each group.

Control	Saline	
G	Gemcitabine	30 mg/kg
T+R	Tocilizumab Reparixin	30 mg/kg 30 mg/kg
½ T+R+G	Tocilizumab Reparixin Gemcitabine	15 mg/kg 15 mg/kg 15 mg/kg
T+R+G	Tocilizumab Reparixin Gemcitabine	30 mg/kg 30 mg/kg 30 mg/kg

4.4.2 Results of *in vivo* study

Over the course of the study, we observed decreased tumor volume in the proposed combination therapy group. As shown in Figure 27, the tumor volume for the T+R+G condition was significantly smaller when compared to the other conditions. As suspected, the T+R treatment had no impact on the tumor volume. The T+R+G group had a decreased tumor volume that was not significant when compared to the gemcitabine group but was significant when compared to the control condition.

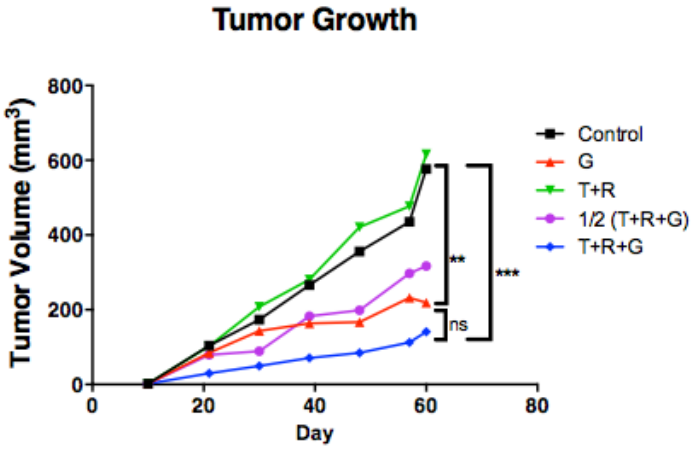

Figure 27: **Comparison of tumor growth for each condition.** Subcutaneous tumor growth over the 60-day study. Tumor volume was calculated using (x,y) measurements from VWR digital calipers (±0.0004mm). Tumors were categorized as spheres or ellipses by calculating the difference between x and y. If x-y < 1mm, the tumor volume was calculated using the volume formula for a sphere. If x-y > 1mm, the tumor volume was calculated using the volume formula for an ellipse.

Tumor volume measurements were taken on the last day of the study (day 60) and mice were sacrificed the following day. A side by side comparison between tumor volume and tumor weight is shown in Figure 28.

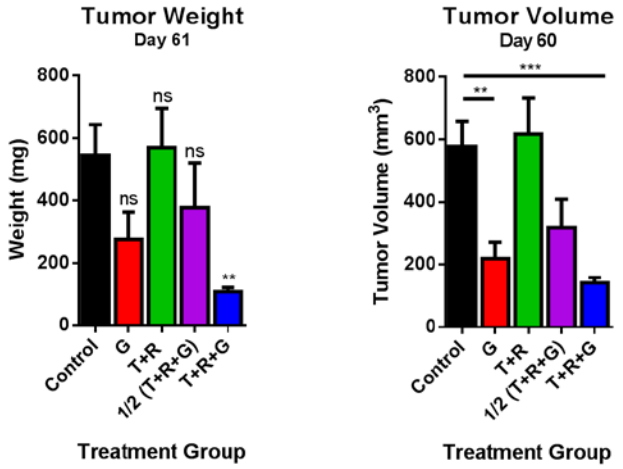

Figure 28: **Final tumor measurements for PDX mouse model.** (A) Weight of excised tumors indicates only T+R+G treatment resulted in statistically significant reduced tumor growth. (B) Final volume measurements, for comparison to the final tumor weight to show accuracy of tumor volume measurements taken throughout the study.

The tumor weight showed statistical significance only in the T+R+G combination group when compared to the control. This data shows that the combination therapy is effective in improving the efficacy of treatment and unexpectedly also improving the anti-proliferative effect of gemcitabine. In Figure 29, visualization of the consistency between tumor size shows that the T+R+G combination resulted in tumor size consistency, which was unexpected. This result suggests that there is a synergistic relationship between the anti-metastatic treatment and anti-proliferation therapy.

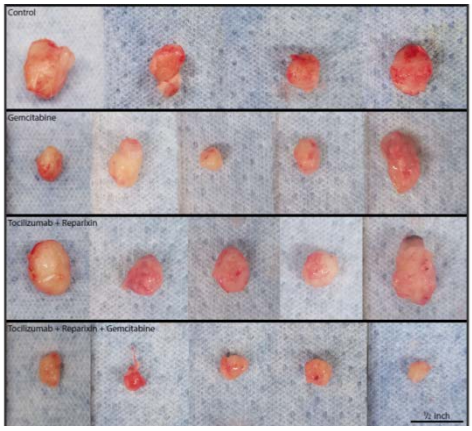

Figure 29: **Excised tumors for each treatment group.** Visualization of tumor size consistency in all the treatment groups suggests the T+R+G combination therapy improves the anti-proliferative effect of gemcitabine. Scale bar (in bottom right of figure) is ½ inch.

To determine if metastatic burden was decreased in the combination therapy, DNA was extracted from harvested organs and analyzed for the expression of H2K, a marker of human genomic material. Our data shows that the combination of T+R+G was effective in preventing metastasis to the lungs and the liver, which is the primary site of metastases in PDAC. The expression of H2K in the T+R+G was comparable to the T+R group, which is expected. The other organs analyzed did not show statistically significant reduced metastatic burden, shown in Figure S7.

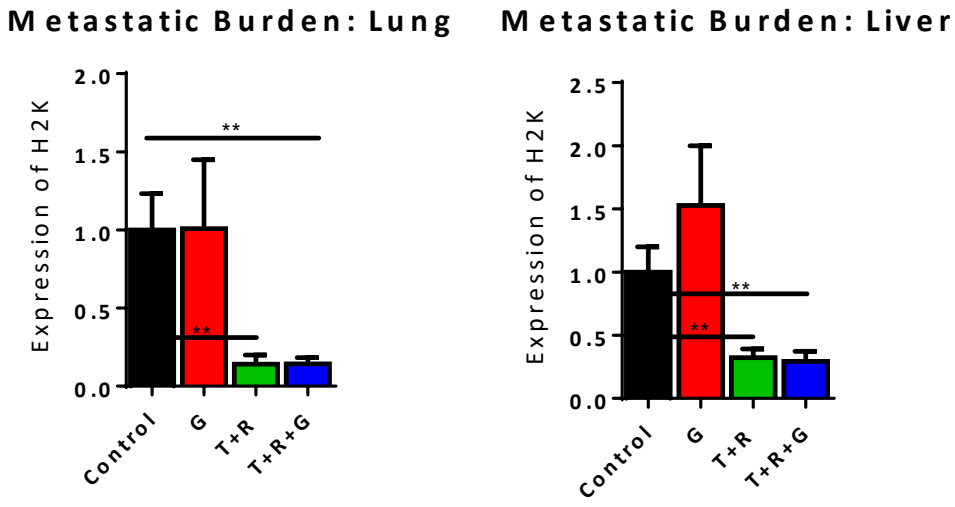

Figure 30: **Metastatic burden to lung and liver is reduced in T+R+G combination therapy group.** (A) shows the relative expression of H2K in the lungs, a marker of human genomic material, is reduced in both the T+R and T+R+G groups. (B) shows the relative expression of H2K in the liver is reduced in both the T+R and T+R+G groups.

The data from the PDX subcutaneous mouse model demonstrates that a combination of tocilizumab and reparixin to target metastasis can be used with an anti-proliferative drug to

increase overall efficacy of treatment. Further studies will be conducted using an orthotopic model to improve relevancy and include the other monotherapy, 5-FU, currently used for treatment of PDAC.

4.5 Future studies

Based on these findings, another *in vivo* study will be conducted in immune-competent mice with an orthotopic tumor implantation to improve accuracy of the metastatic spread. The subcutaneous model in immune-suppressed mice has shown efficacy of our proposed combination therapy, but further validation is needed to make progress towards a clinical trial. More *in vitro* studies will be conducted to better understand the paracrine pathway that enables cells to sense IL-6 and IL-8 secretions and initiate the intracellular cascade that promotes enhanced migratory phenotypes.

5 Exploring unconventional metastasis

As mentioned previously, metastasis is defined as the spread of cancer from the primary tumor site through the circulatory or lymphatic systems to a secondary site. This mechanism of metastasis has been studied extensively, allowing researchers to study the various signaling pathways and proteins that are involved in this process. However, this is not the only mechanism by which tumor cells metastasize to a secondary site. Cancers arising in the peritoneal cavity can bypass the process of intravasation and extravasation by disseminating into the peritoneal fluid and migrating to a secondary site. Both ovarian and pancreatic cancer cells can metastasize via this mechanism, which is not well understood. We wanted to explore this other mechanism of metastasis, since peritoneal cancers are some of the deadliest.

5.1 Metastasis and the omentum

In ovarian cancer, the omentum is the most common site of metastasis, and other cancers arising in the peritoneal cavity often metastasize to the omentum as well.[33] The omentum is a complex fatty membrane that lies on top of the abdominal organs, functioning as the "policeman of the abdomen" due to its immune response when pathogens are present in the peritoneal cavity.[34] The mechanism by which cancer cells metastasize to omentum is not well understood, but numerous studies have shown that cancer cells can migrate directly through the peritoneal fluid,

bypassing the mechanism outlined earlier that involves the circulatory or lymphatic systems.[35-37] Lengyel *et al* have studied the impact of adipocytes and mesothelial cells on ovarian cancer cell behavior, but their models lack some important ECM components that we suspect are necessary to map the mechanism by which cancer cells are able to metastasize within the peritoneal cavity and why the omentum is one of the most common sites of metastases for abdominal cancers. With this basis, we have begun to explore the mechanism of metastasis utilizing a novel co-culture system that includes many of the native and specific components.

5.2 Development of a novel co-culture system

Previous studies conducted by Lengyel *et al* used a co-culture system of mesothelial cells, which are present on the surface of the omentum, and adipocytes, which comprise the inner fatty layers. However, the models used in previous studies look at cell invasion in 3D matrices and quantified invasion by fluorescently labeling ovarian cancer cells and quantifying the number of cells that successfully migrated to the mesothelial layer. Other models quantified proliferation and adhesion to various ECM variations, but none have studied how the omentum affects the migratory phenotypes of these cells.[35-37]

With this basis, we proposed a novel co-culture system that will allow us to study the impact the omentum has on the migratory phenotypes of ovarian and pancreatic cancer cells. This novel system recapitulates the ECM utilizing a type I collagen matrix and fresh human omental tissue. A schematic of the proposed system is shown in Figure 31.

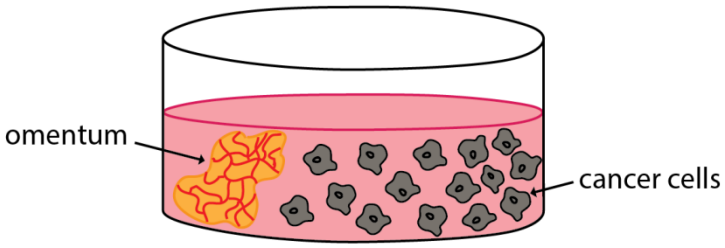

Figure 31. **Omentum co-culture system.** Proposed 3D system to study the impact of omentum on cancer cell migration and phenotypes. Omentum tissue and cells will be embedded in a collagen I matrix.

By embedding a piece of fresh human omentum into a collagen I matrix, we can co-culture cancer cells with the

tissue and track how the cells morphology and migratory patterns change in the presence of all the components of the omentum. As mentioned previously, the omentum is an extremely complex tissue, and keeping the tissue intact allows us to simulate a physiologically relevant ECM to track cancer cell migration and phenotypic shifts.

5.3 Future studies

We have conducted preliminary studies with this novel co-culture system and observed a surprising phenomenon. We will continue to explore the mechanism of metastasis within the peritoneal cavity, with an initial focus on the impact of the omentum on ovarian and pancreatic cancer cell migratory phenotypes.

6 Materials and methods

6.1 TNBC and E-cadherin project

Cell culture

Human breast carcinoma MDA-MB-231 cells (ATCC) were cultured in Dulbecco's modified Eagle's medium (DMEM, Sigma Aldrich) supplemented with 10% (v/v) fetal bovine serum (FBS, Corning) and 1% Penicillin-Streptomycin (Corning). The cells were maintained in at 37°C and 5% CO_2 in a humidified incubator during cell culture and during live-cell microscopy studies.

Lentiviral expression constructs[18]

The lentiviral vector of enhanced green fluorescent protein (EGFP; pCS-CG) was purchased from Addgene (Cambridge, MA). The lentiviral vector of lifeact-EGFP and E-cadherin-EGFP were generated from pCS-CG. The sequence of lifeact peptide or full-length E-cadherin was cloned upstream of EGFP between the Nhe1 and Age 1 sites of pCS-CG to generate EGFP-fused protein. The aE-catenin shRNA vector was generated as described before. Briefly, the sequence 50-GGACCTGCTTTCG GAGTACAT-30 targeting aE-catenin was cloned downstream of the H1 promoter between the MluI and ClaI sites in pLVTHM lentiviral vector (Addgene).

Lentivirus production and transduction[18]

A second-generation lentivirus was produced as described previously (11). Briefly, MDA-MB-231 cells (ATCC) were transiently co-transfected with three plasmids (lentiviral vector, DR 8.91, and pMDG-VSVG) using the standard calcium phosphate precipitation method. After 22–24 h of transfection, the medium was replaced with fresh medium. The lentiviral particles were harvested 24 h later, immediately filtered through 0.45 mm filter (Millipore) to remove cells debris, and then stored at 80°C. For transduction, $1*10^5$ cells in a 35-mm culture dish were repeatedly transduced with lentivirus with 8 mg/ml polybrene to reach high transduction (>80%) to generate MDA-MB-231 + E-cadherin.

Double-layered spheroid model

A double layered spheroid model was generated with matrigel (Corning) and rat tail type I (Corning). Cells were trypsinized, pelleted, and re-suspended in matrigel such that the final concentration of cells was 50,000 per 0.6 uL. Oil columns were prepared in 10 uL pipette tips without a filter/barrier. First, 10uL of media was aspirated and tips were placed back into the box. Then, 40uL of sterile biological grade mineral oil (Sigma Aldrich) was added to the top of the pipette tip. To generate the first layer, 0.6 uL of the matrigel/cell mixture is pipette into each prepared oil column. Incubate at 37°C for 1 hr.

After 1 hr incubation, the matrigel layered sphere is formed. With a cut 200uL pipette tip, spheroids were taken out of the oil column and put into an Eppendorf tube of media. The spheroids should sink to the bottom of the Eppendorf. To generate the second layer, a 2mg/mL collagen I gel was mixed as previously described by Frayley *et al.*[16] Matrigel layered spheroids were carefully dropped into the collagen gel mixture. Using a cut tip, 6 uL of collagen mixture + spheroid was aspirated and dropped into the oil column from earlier. The second layer was incubated for 1 hr at 37°C. After the second layer set, the spheroids were washed again in media and then plate in a 96 well round-bottom dish and suspended in media.

Quantifying double-layered spheroid volume

Inner and outer layers were manually traced using NIS Elements software to generate a radius measurement. Volume of inner and total spheroid was calculated using volume for a sphere

formula: $V = \frac{4}{3}\pi r^3$. To calculate the volume of the collagen layer (stroma), the inner volume was subtracted from the total volume.

mRNA extraction

Spheroids were generated and then incubated for 24hrs in fresh media. After 24hrs, spheroids were harvested and washed 3x in DPBS (Corning). To isolate mRNA,TriZol reagent (Invitrogen) was added to the spheroids and then vortexed until completely dissolved. Direct-zol Mini Prep kit (Zymo research) reagents and protocol were used to finish the RNA extraction process.

cDNA synthesis and qPCR

cDNA was synthesized using Bio-Rad cDNA iScript kit following the protocol to make 1000ng/uL of cDNA for a total reaction volume of 20uL. qPCR was conducted with iTaq-SYBR Green (Bio-Rad) using the Bio-Rad CFX CFX384 Touch Real-Time PCR Detection System. Primers were obtained from Integrated DNA Technologies. A complete list of primers and sequences is included in Supplementary Table 1.

Inhibitor studies

Inhibitor studies were conducted using 3DLTS system described above. Experiments were carried out for 1 week and imaged every day using phase microscopy. NIS Elements was used to manually trace the inner and outer layers of the spheroids to generate a radius measurement for calculations. Volume calculations were used to track the size of both the inner sphere (cells) and the outer sphere (stroma). Inhibitors were obtained from Sellechem and fresh or conditioned media was added on the day the spheroids were generated and not changed during the week-long experiment.

Protein extraction and assay (western blot)

A clear sample buffer containing SDS was used to lyse 10-15 spheroids. Samples were sonicated to manually break up the gel layers and dissolve the collagen and matrigel. Samples were then heated at 100°C for 5 minutes to completely denature the protein. Protein samples were stored in -80°C freezer until ready for use. A loading buffer made from 2x Laemlli (Biorad) was prepared

with the instructed amount of beta mercaptoethanol and added in a one-to-one ratio to the protein samples. Bio-rad mini protean gels with a 4-15% gradient were used for gel electrophoresis. Transblot Turbo packs from Bio-rad were used for transfer from gel to PVDF membrane. Antibodies were purchased from Cell Signaling Technology and recommended dilutions for the primary and secondary antibodies were used in blocking. Blots were imaged using Bio-Rad imager and bands were quantified using ImageJ.

6.2 PDAC and IL-6/IL-8 signaling project

Cell culture

Human pancreatic ductal adenocarcinoma cells Panc-1 (ATCC) were cultured in DMEM (Sigma Aldrich) supplemented with 10% (v/v) FBS (Corning) and 1% Penicillin-Streptomycin (Corning). Human pancreatic ductal adenocarcinoma cells Capan-1 (ATCC) were cultured in IMDM (ATCC) supplemented with 20% FBS (Corning). The cells were maintained in at 37°C and 5% CO_2 in a humidified incubator during cell culture and during live-cell microscopy studies.

3D collagen I matrix for single cell migration studies

PDAC cell lines Panc-1 and Capan-1 were embedded in 2mg/mL type I collagen gel as described previously by Fraley *et al*.[16] Cell suspensions containing 5,000 to 75,000 cells in a 1:1 (v/v) ratio of cell culture media and reconstitution buffer were mixed with soluble rat-tail type I collagen (Corning) to obtain a final collagen concentration of 2mg/mL. After adding the appropriate collagen volume, a calculated volume 1M NaOH was added quickly to have a final solution pH of approximately 7. The cell-suspension gel mixture was added to 24-well coverslip-bottom cell culture dish on a plate heater set to 37°C for approximately 5 minutes and then transferred to an incubator maintained at 37°C to allow for polymerization. Fresh media was added 1 h after gels were placed in the incubator and imaged for approximately 16 h.

mRNA extraction

PDAC cell lines were seeded in high and low densities in 2mg/mL collagen I matrices in a 6-well plate coverslip-bottom cell culture dish. High density wells received conditioned medium or control medium and then were harvested after 24-hour incubation. Collagenase (Corning) was prepared in DPBS (Corning) for a final concentration of 2mg/mL. An equal volume of collagenase was added to the total collagen volume for each condition into conical tubes and incubated for 1 h in a humidified incubator at 37°C with 5% CO_2. After collagen was dissolved, the cells were pelleted via centrifugation and re-suspended in 2-3mL of DPBS to remove any residual collagenase and media serum. Cells were pelleted again via centrifugation and DPBS was removed to begin the RNA extraction process. mRNA was extracted from the cell pellet using TriZol (Invitrogen). Direct-zol RNA mini-prep kit (Zymo Research) using the supplied reagents. Absorbance values of 260/280 (acceptable range: 2.2-1.7) and 260/230 (acceptable range: below 2.3) were used for quality control purposes.

Secretomic analysis (ELISA)

PDAC cells were seeded in 2mg/mL collagen I gels at varying cell densities and media was harvested after 24 hours of incubation and centrifuged. ELISA kits were obtained from R&D systems and experiment was carried out using supplied reagents and protocol.

PDX mouse model

Studies using 6-8 week old NSG (NOD SCID Gamma) mice were carried out according to protocols approved by the Johns Hopkins University Animal Care and Use Committee in accordance with the NIH Guide for the Care and Use of Laboratory Animals. All mice were housed at a temperature of 25°C under a 12 hr dark/light cycle. NSG mice were obtained from Jackson Laboratories and were implanted with tumor cells subcutaneously by Jackson Laboratories before arrival at the mouse facilities at the Johns Hopkins University. Tocilizumab and saline were obtained from Genentech, Reparixin was obtained from Med Chem Express, and Gemcitabine was obtained from Sagent. Injections began 11 days after tumor implantation. The control group mice were injected with 100 uL saline. Treatment groups were injected with 100 uL gemcitabine (30 mg/kg), 100 uL of tocilizumab and reparixin combination (both 30mg/kg), 200 uL of tocilizumab, reparixin, and gemcitabine (all 30 mg/kg), or 100uL of tocilizumab, reparixin,

and gemcitabine (all 15 mg/kg). Mice were injected every three days for approximately 9 weeks (61 days). Tumors were measured in two dimensions (x and y) with calipers on the same day as injections and mice were weighed once a week. Tumors were categorized as spheres or ellipses by calculating the difference between x and y. If x-y < 1mm, the tumor volume was calculated using the volume formula for a sphere. If x-y > 1mm, the tumor volume was calculated using the volume formula for an ellipse. Mice were sacrificed using isoflurane and cervical dislocation. Primary tumors were excised and weighed. The liver, lungs, lymph nodes, spleen, pancreas, kidneys, brain were also harvested for mRNA/qPCR studies.

Processing of harvested mouse tissues

All tissues were fixed in formalin to be sectioned and stained. The primary tumors were not stained but sectioned for future studies. All tissues except the lymph nodes were H&E stained, and lymph nodes were stained with pan cytokeratin. RNA and protein were extracted from primary tumors using All-Prep RNA/Protein Kit (Qiagen) using the supplied reagents and protocol. DNA was extracted from all other organs using Invitrogen PureLink Genomic DNA Mini-kit (Thermo Fischer Scientific). To test for metastatic burden, qPCR was run to test for the expression of the H2K gene, which is a marker of human genomic material.

Gene sequences for qPCR

Beta actin was chosen as the housekeeping gene for normalization.. Primer mix included forward and reverse of both human and mouse DNA primers for B-actin.

B-actin PDAC	Fwd	AGATCAAGATCATTGCTCCTCCT
B-actin PDAC	Rvs	ACGCAGCTCAGTAACAGTCC
B-actin mouse 1	Fwd	ATGAGCTGCCTGACGGCCAGGTCATC
B-actin mouse 1	Rvs	TGGTACCACCAGACAGCACTGTGTTG
H2K	Fwd	CCAGTTCATTCACATCATCAG
H2K	Rvs	CTTACACGAGGTCACATAGC

Statistics

The mean values of data presented ± SEM were calculated and plotted using GraphPad Prism software (GraphPad Software). One-way ANOVA test and T-TEST were used to determine statistical significance between data sets. Statistical significance presented on the graphs uses the Michelin grade scale:

****	P<0.001
***	P <0.01
**	P<0.02
*	P<0.05

References

1 Weinberg RA. The biology of cancer. Garland Science: New York.

2 Society., A. C., 2017, C. F. F., . & 2017, A. A. C. S.

3 BreastCancer.Org. *What Is Triple-Negative Breast Cancer?*

4 Steeg, P. S. Targeting metastasis. *Nature Reviews Cancer* **16**, 201, doi:10.1038/nrc.2016.25 (2016).

5 Jayatilaka, H. *et al.* Synergistic IL-6 and IL-8 paracrine signalling pathway infers a strategy to inhibit tumour cell migration. *Nature Communications* **8**, 15584, doi:10.1038/ncomms15584 https://www.nature.com/articles/ncomms15584#supplementary-information (2017).

6 Adamska, A., Domenichini, A. & Falasca, M. Pancreatic Ductal Adenocarcinoma: Current and Evolving Therapies. *International Journal of Molecular Sciences* **18**, 1338, doi:10.3390/ijms18071338 (2017).

7 Wirtz, D., Konstantopoulos, K. & Searson, P. C. The physics of cancer: the role of physical interactions and mechanical forces in metastasis. *Nature Reviews. Cancer* **11**, 512-522, doi:10.1038/nrc3080 (2011).

8 Chaffer, C. L. & Weinberg, R. A. A Perspective on Cancer Cell Metastasis. *Science* **331**, 1559-1564, doi:10.1126/science.1203543 (2011).

9 Polyak, K. & Weinberg, R. A. Transitions between epithelial and mesenchymal states: acquisition of malignant and stem cell traits. *Nature Reviews Cancer* **9**, 265, doi:10.1038/nrc2620 (2009).

10 Giri, A. *et al.* The Arp2/3 complex mediates multigeneration dendritic protrusions for efficient 3-dimensional cancer cell migration. *The FASEB Journal* **27**, 4089-4099, doi:10.1096/fj.12-224352 (2013).

11 Frantz, C., Stewart, K. M. & Weaver, V. M. The extracellular matrix at a glance. *Journal of Cell Science* **123**, 4195-4200, doi:10.1242/jcs.023820 (2010).

12 Thiery, J. P., Acloque, H., Huang, R. Y. J. & Nieto, M. A. Epithelial-Mesenchymal Transitions in Development and Disease. *Cell* **139**, 871-890, doi:https://doi.org/10.1016/j.cell.2009.11.007 (2009).

13 Fraley, S. I. *et al.* Three-dimensional matrix fiber alignment modulates cell migration and MT1-MMP utility by spatially and temporally directing protrusions. *Scientific Reports* **5**, 14580, doi:10.1038/srep14580 https://www.nature.com/articles/srep14580#supplementary-information (2015).
14 Wu, P.-H., Giri, A., Sun, S. X. & Wirtz, D. Three-dimensional cell migration does not follow a random walk. *Proceedings of the National Academy of Sciences of the United States of America* **111**, 3949-3954, doi:10.1073/pnas.1318967111 (2014).
15 Chu, K., Boley, K. M., Moraes, R., Barsky, S. H. & Robertson, F. M. The Paradox of E-Cadherin: Role in response to hypoxia in the tumor microenvironment and regulation of energy metabolism. *Oncotarget* **4**, 446-462 (2013).
16 Sebba, A. Tocilizumab: The first interleukin-6-receptor inhibitor. *American Journal of Health-System Pharmacy* **65**, 1413-1418, doi:10.2146/ajhp070449 (2008).
17 Opfermann, P. *et al.* A pilot study on reparixin, a CXCR1/2 antagonist, to assess safety and efficacy in attenuating ischaemia–reperfusion injury and inflammation after on-pump coronary artery bypass graft surgery. *Clinical and Experimental Immunology* **180**, 131-142, doi:10.1111/cei.12488 (2015).
18 van Roy, F. & Berx, G. The cell-cell adhesion molecule E-cadherin. *Cellular and Molecular Life Sciences* **65**, 3756-3788, doi:10.1007/s00018-008-8281-1 (2008).
19 Onder, T. T. *et al.* Loss of E-Cadherin Promotes Metastasis via Multiple Downstream Transcriptional Pathways. *Cancer Research* **68**, 3645-3654, doi:10.1158/0008-5472.can-07-2938 (2008).
20 Rodriguez, F. J., Lewis-Tuffin, L. J. & Anastasiadis, P. Z. E-cadherin's dark side: possible role in tumor progression. *Biochimica et Biophysica Acta* **1826**, 23-31, doi:10.1016/j.bbcan.2012.03.002 (2012).
21 Davoli, T. *et al.* Cumulative Haploinsufficiency and Triplosensitivity Drive Aneuploidy Patterns to Shape the Cancer Genome. *Cell* **155**, 948-962, doi:10.1016/j.cell.2013.10.011 (2013).
22 Valencia, A. M. J. *et al.* Collective cancer cell invasion induced by coordinated contractile stresses. *Oncotarget* **6**, 43438-43451 (2015).
23 Shamir, E. R. & Ewald, A. J. Three-dimensional organotypic culture: experimental models of mammalian biology and disease. *Nature reviews. Molecular cell biology* **15**, 647-664, doi:10.1038/nrm3873 (2014).
24 Fatehullah, A., Tan, S. H. & Barker, N. Organoids as an in vitro model of human development and disease. *Nature Cell Biology* **18**, 246, doi:10.1038/ncb3312 (2016).
25 Dhillon, A. S., Hagan, S., Rath, O. & Kolch, W. MAP kinase signalling pathways in cancer. *Oncogene* **26**, 3279, doi:10.1038/sj.onc.1210421 (2007).
26 Polakis, P. Wnt Signaling in Cancer. *Cold Spring Harbor Perspectives in Biology* **4**, a008052, doi:10.1101/cshperspect.a008052 (2012).
27 Harvey, K. F., Zhang, X. & Thomas, D. M. The Hippo pathway and human cancer. *Nature Reviews Cancer* **13**, 246, doi:10.1038/nrc3458 https://www.nature.com/articles/nrc3458#supplementary-information (2013).
28 Irvine, K. D. Integration of intercellular signaling through the Hippo pathway. *Seminars in cell & developmental biology* **23**, 812-817, doi:10.1016/j.semcdb.2012.04.006 (2012).
29 Henderson, Y. C., Chen, Y., Frederick, M. J., Lai, S. Y. & Clayman, G. L. MEK Inhibitor PD0325901 Significantly Reduces the Growth of Papillary Thyroid Carcinoma Cells In

vitro and In vivo. *Molecular cancer therapeutics* **9**, 1968-1976, doi:10.1158/1535-7163.mct-10-0062 (2010).
30 Haura, E. B. *et al.* A Phase II Study of PD-0325901, an Oral MEK Inhibitor, in Previously Treated Patients with Advanced Non–Small Cell Lung Cancer. *Clinical Cancer Research* **16**, 2450 (2010).
31 de Sousa Cavalcante, L. & Monteiro, G. Gemcitabine: Metabolism and molecular mechanisms of action, sensitivity and chemoresistance in pancreatic cancer. *European Journal of Pharmacology* **741**, 8-16, doi:https://doi.org/10.1016/j.ejphar.2014.07.041 (2014).
32 Longley, D. B., Harkin, D. P. & Johnston, P. G. 5-Fluorouracil: mechanisms of action and clinical strategies. *Nature Reviews Cancer* **3**, 330, doi:10.1038/nrc1074 (2003).
33 Krist Lambert, F. G. *et al.* Cellular composition of milky spots in the human greater omentum: An immunochemical and ultrastructural study. *The Anatomical Record* **241**, 163-174, doi:10.1002/ar.1092410204 (1995).
34 Meza-Perez, S. & Randall, T. D. Immunological Functions of the Omentum. *Trends in Immunology* **38**, 526-536, doi:10.1016/j.it.2017.03.002 (2017).
35 Kenny, H. A., Nieman, K. M., Mitra, A. K. & Lengyel, E. The First Line of Abdominal Metastatic Attack: Breaching the Mesothelial Cell Layer. *Cancer discovery* **1**, 100-102, doi:10.1158/2159-8290.cd-11-0117 (2011).
36 Lengyel, E. Ovarian Cancer Development and Metastasis. *The American Journal of Pathology* **177**, 1053-1064, doi:10.2353/ajpath.2010.100105 (2010).
37 Nieman, K. M. *et al.* Adipocytes promote ovarian cancer metastasis and provide energy for rapid tumor growth. *Nature medicine* **17**, 1498-1503, doi:10.1038/nm.2492 (2011).
38 Gyorffy B, Lanczky A, Eklund AC, Denkert C, Budczies J, Li Q, Szallasi Z. An online survival analysis tool to rapidly assess the effect of 22,277 genes on breast cancer prognosis using microarray data of 1809 patients, Breast Cancer Res Treatment, 2010 Oct;123(3):725-31.

7 Supplementary figures and data

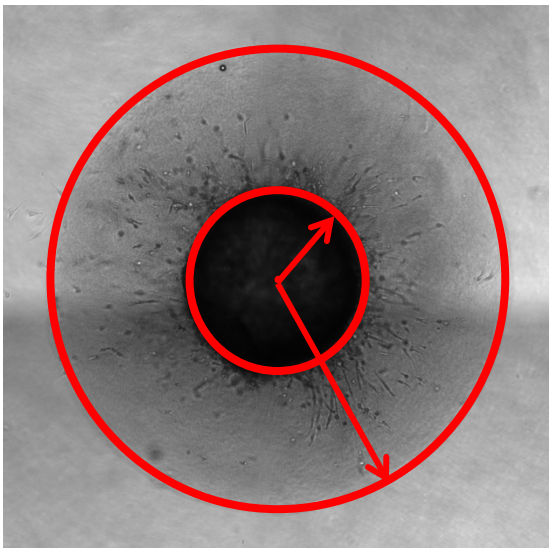

Figure S1:**Spheroid measurement graphic.** Red annotations show how the spheroid measurements were taken using NIS elements.

As outlined in the methods section, the spheroid volume measurements were calculated by manually tracing the inner and outer spheres in NIS Elements to generate a radius measurement.

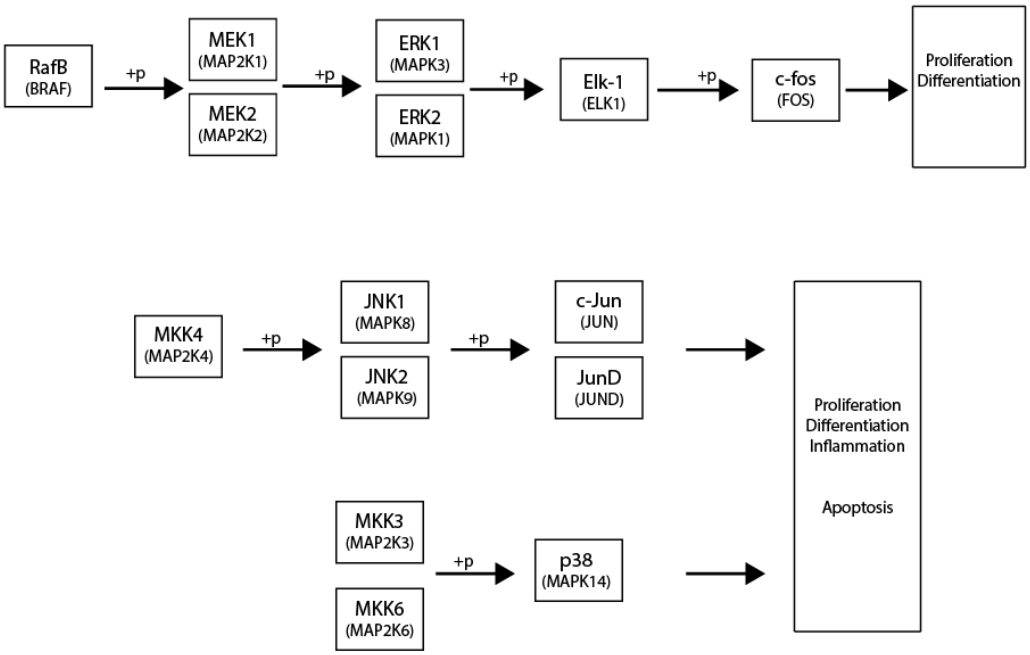

Figure S2: **MAPKinase signaling pathway**. Simplified schematic of the individual cascades within the complex MAPKinase pathway. Boxes contain the protein name and the gene name that encodes the protein in parentheses.

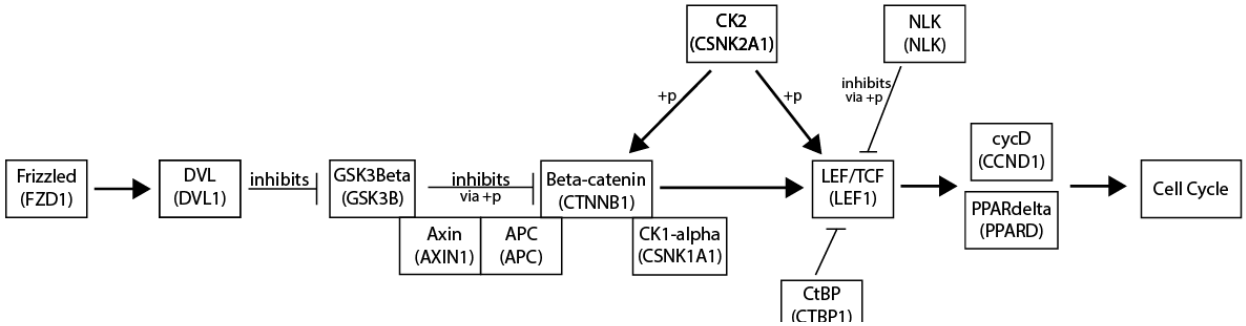

Figure S3: **WNT signaling pathway.** Simplified schematic of the WNT canonical pathway. Boxes contain the protein name and the gene name that encodes the protein in parentheses.

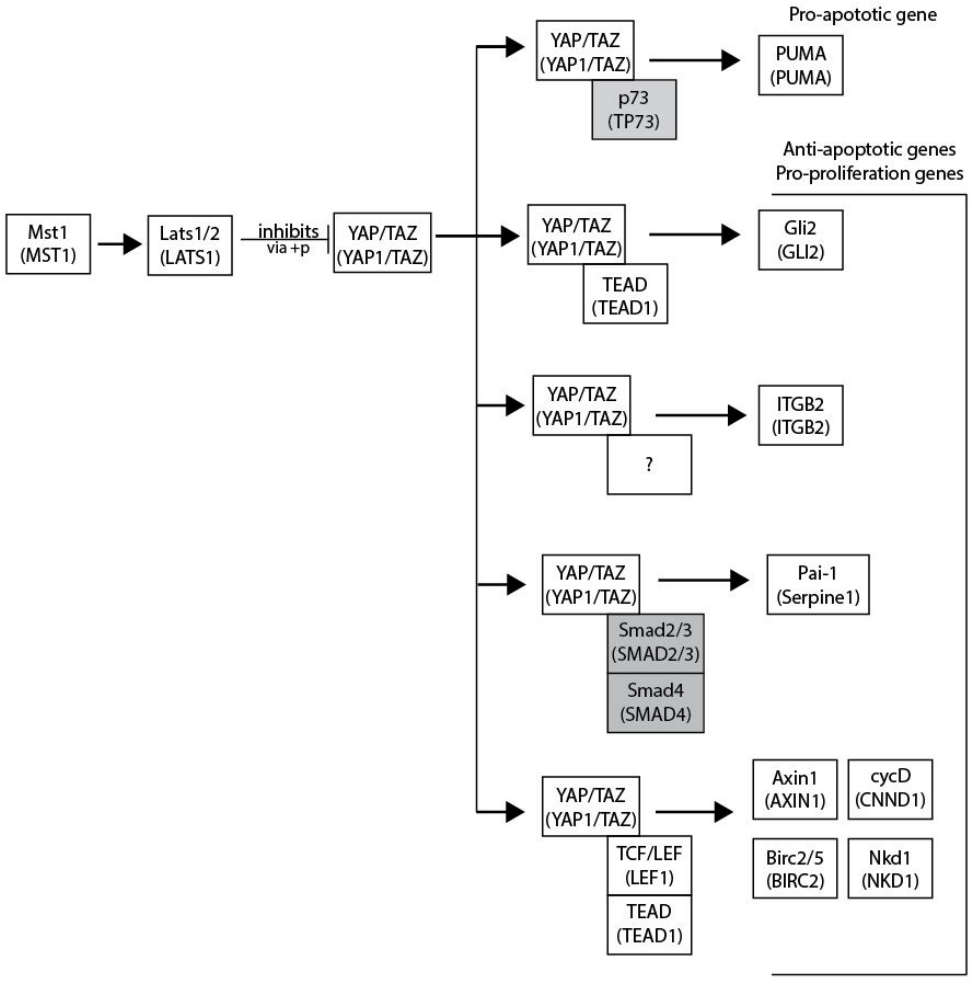

Figure S4: **HIPPO signaling pathway.** Simplified schematic of the HIPPO signaling pathway. Boxes contain the protein name and the gene name that encodes the protein in parentheses.

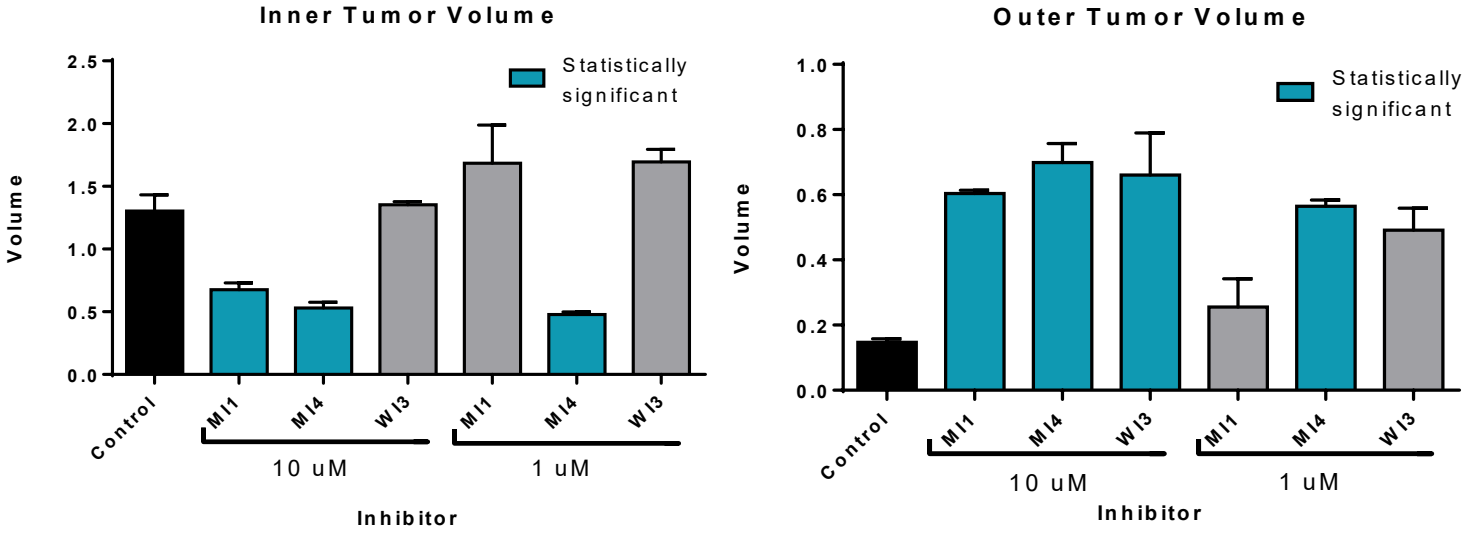

Figure S6: **Proliferation fold increase for MDA-MB-231 WT and MDA-MB-231 +E-cadherin in both 2D and 3DLTS**. In 2D condition, there is no difference between the fold increase in the cells over-expressing E-cadherin

bFigure S5: **10uM and 1uM inhibitor screening.** Inhibitor screening of the inhibitors selected after the initial 10uM

lcscreening experiment. Only MI4 was able to maintain the tumor stroma volume and prevent the inner spheroid volume from progressing as quickly when treated with the lower concentration.

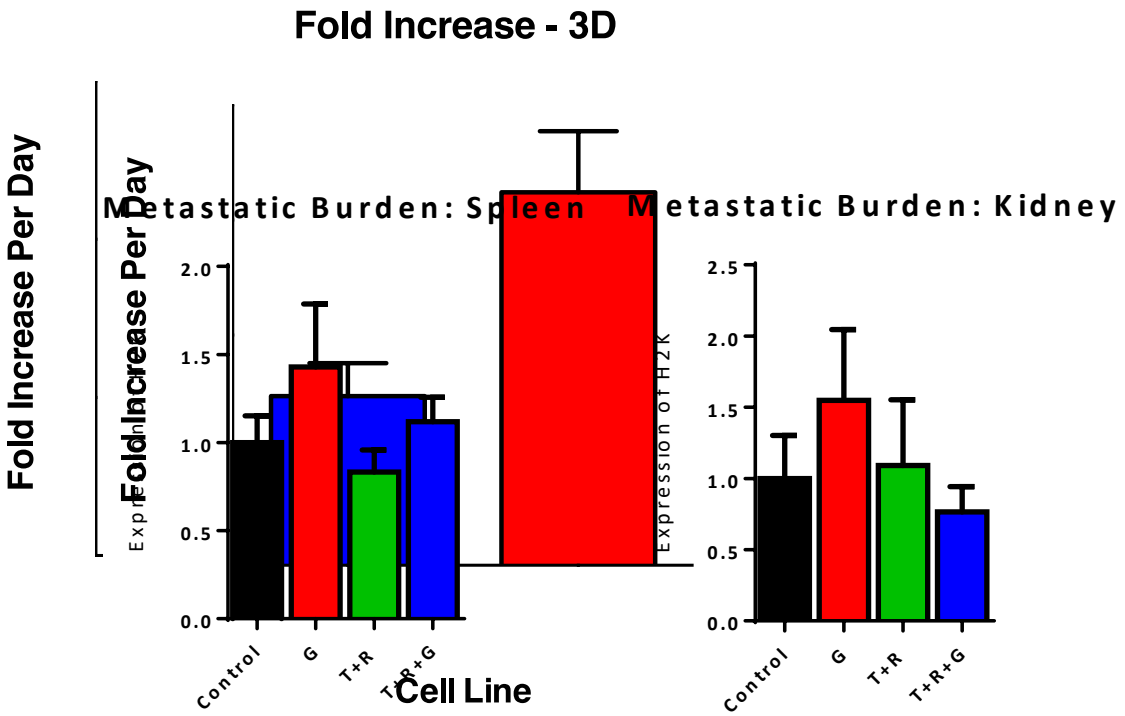

Figure S7: **Metastatic burden analysis on spleen and kidneys**. Expression of H2K was evaluated to quantify the metastatic burden in the different treatment groups. All were NS when compared to the control.

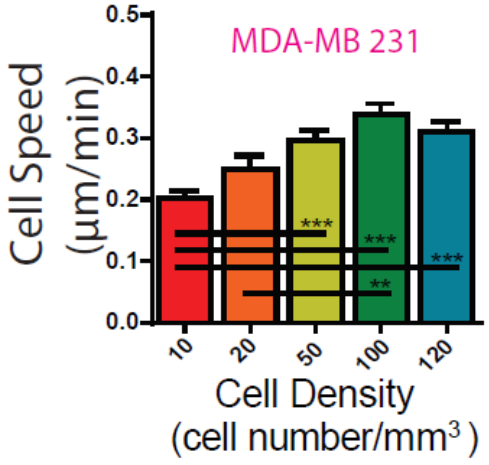

Figure S8: **Cell density dependent speed in MDA-MB-231.** As cell density is increased, cell speed increases. There is a point at which the effect plateaus, as seen for 100 to 120 cell number/mm^3.[5]

Supplementary Table 1:

MAPK Pathway Gene Primer List

Primer	Sequence
AKT1 FWD	AGCGACGTGGCTATTGTGAAG
AKT1 RVS	GCCATCATTCTTGAGGAGGAAGT
ATF2 FWD	AATTGAGGAGCCTTCTGTTGTAG
ATF2 RVS	CATCACTGGTAGTAGACTCTGGG
DAXX FWD	GATACCTTCCCTGACTATGGGG
DAXX RVS	GTAACCTGATGCCCACATCTC
ELK1 FWD	CTGCCTCCTAGCATTCACTTC
ELK1 RVS	GCTGCCACTGGATGGAAACT
FOS FWD	CCGGGGATAGCCTCTCTTACT
FOS RVS	CCAGGTCCGTGCAGAAGTC
GREB1 FWD	ATGGGAAATTCTTACGCTGGAC
GREB1 RVS	CACTCGGCTACCACCTTCT
JUN FWD	TCCAAGTGCCGAAAAAGGAAG
JUN RVS	CGAGTTCTGAGCTTTCAAGGT
JUND FWD	TCATCATCCAGTCCAACGGG
JUND RVS	TTCTGCTTGTGTAAATCCTCCAG

MAP2K1 FWD	CAATGGCGGTGTGGTGTTC
MAP2K1 RVS	GATTGCGGGTTTGATCTCCAG
MAP2K2 FWD	AGGTCCTGCACGAATGCAA
MAP2K2 RVS	CGTCCATGTGTTCCATGCAA
MAP2K3 FWD	GAGGGAGACGTGTGGATCTG
MAP2K3 RVS	CCGCACGATAGACACAGCAAT
MAP2K4 FWD	TGCAGGGTAAACGCAAAGCA
MAP2K4 RVS	CTCCTGTAGGATTGGGATTCAGA
MAP2K5 FWD	CCGGACCCTCTCAACACAG
MAP2K5 RVS	ATGACCAAGAGTGTCCCGATA
MAP2K6 FWD	AAACGGCTACTGATGGATTTGG
MAP2K6 RVS	CAGTGCGCCATAAAAGGTGAC
MAPK1 FWD	TCACACAGGGTTCCTGACAGA
MAPK1 RVS	ATGCAGCCTACAGACCAAATATC
MAPK10 FWD	CAGATGGAATTAGACCATGAGCG
MAPK10 RVS	TCAATGTGCAATCAGACTTGACT
MAPK12 FWD	AGTGGCTTTTACCGCCAGG
MAPK12 RVS	GACTGGAAGGGCCGATACAG
MAPK13 FWD	TGAGCCGACCCTTTCAGTC
MAPK13 RVS	AGCCCAATGACGTTCTCATGC
MAPK14 FWD	TCAGTCCATCATTCATGCGAAA
MAPK14 RVS	AACGTCCAACAGACCAATCAC
MAPK3 FWD	CTACACGCAGTTGCAGTACAT
MAPK3 RVS	CAGCAGGATCTGGATCTCCC
MAPK8 FWD	TCTGGTATGATCCTTCTGAAGCA
MAPK8 RVS	TCCTCCAAGTCCATAACTTCCTT
MAPK9 FWD	GAAACTAAGCCGTCCTTTTCAGA
MAPK9 RVS	TCCAGCTCCATGTGAATAACCT
MAX FWD	CAATCTGCGGCTGACAAACG
MAX RVS	GCACTTGACCTCGCCTTCT
TRAF2 FWD	CCTTCCCAGATAATGCTGCCC
TRAF2 RVS	GCTCTCGTATTCTTTCAGGGTC

Supplementary Table 2:

WNT Pathway Gene Primer List

Primer	Sequence
APC FWD	AAGCATGAAACCGGCTCACAT
APC RVS	CATTCGTGTAGTTGAACCCTGA
AXIN1 FWD	GGTTTCCCCTTGGACCTCG

AXIN1 RVS	CCGTCGAAGTCTCACCTTTAATG
BTRC FWD	TGCCCAAGCAACGGAAACT
BTRC RVS	GCCCATGTTGGTAATGACACA
CCND1 FWD	GCTGCGAAGTGGAAACCATC
CCND1 RVS	CCTCCTTCTGCACACATTTGAA
CSNK1A1 FWD	AGTGGCAGTGAAGCTAGAATCT
CSNK1A1 RVS	CGCCCAATACCCATTAGGAAGTT
CSNK2A1 FWD	CGAGTTGCTTCCCGATACTTC
CSNK2A1 RVS	ACTTGCCAGCATACAACCCAA
CTBP1 FWD	CGACCCTTACTTGTCGGATGG
CTBP1 RVS	TTGACGGTGAAGTCGTTGATG
CTNNB1 FWD	AGCTTCCAGACACGCTATCAT
CTNNB1 RVS	CGGTACAACGAGCTGTTTCTAC
DVL1 FWD	GAGGGTGCTCACTCGGATG
DVL1 RVS	GTGCCTGTCTCGTTGTCCA
FZD1 FWD	ATCTTCTTGTCCGGCTGTTACA
FZD1 RVS	GTCCTCGGCGAACTTGTCATT
GSK3B FWD	GGCAGCATGAAAGTTAGCAGA
GSK3B RVS	GGCGACCAGTTCTCCTGAATC
HDAC1 FWD	CTACTACGACGGGGATGTTGG
HDAC1 RVS	GAGTCATGCGGATTCGGTGAG
LEF1 FWD	AGAACACCCCGATGACGGA
LEF1 RVS	GGCATCATTATGTACCCGGAAT
NLK FWD	CCAACCTCCACACATTGACTATT
NLK RVS	ACTTTGACATGATCTGAGCTGAG
PPARD FWD	GCCTCTATCGTCAACAAGGAC
PPARD RVS	GCAATGAATAGGGCCAGGTC
PPP2CA FWD	GTTCGTTACCGTGAACGCATC
PPP2CA RVS	TGGCGAGAGACCACCATGT
WIF1 FWD	TCTCCAAACACCTCAAAATGCT
WIF1 RVS	GACACTCGCAGATGCGTCT
WNT1 FWD	CGATGGTGGGGTATTGTGAAC
WNT1 RVS	CCGGATTTTGGCGTATCAGAC
WNT11 FWD	GGAGTCGGCCTTCGTGTATG
WNT11 RVS	GCCCGTAGCTGAGGTTGTC
WNT5A FWD	ATTCTTGGTGGTCGCTAGGTA
WNT5A RVS	CGCCTTCTCCGATGTACTGC

Supplementary Table 3:

HIPPO Pathway Gene Primer List

Lable	Name	Sequence
Hs1	PUMA delta FWD	GCCAGATTTGTGAGACAAGAGG
Hs2	PUMA delta RVS	CAGGCACCTAATTGGGCTC
Hs3	CTGF FWD	CAGCATGGACGTTCGTCTG
Hs4	CTGF RVS	AACCACGGTTTGGTCCTTGG
Hs5	GLI2 FWD	CTGCCTCCGAGAAGCAAGAAG
Hs6	GLI2 RVS	GCATGGAATGGTGGCAAGAG
Hs7	AREG FWD	GTGGTGCTGTCGCTCTTGATA
Hs8	AREG RVS	CCCCAGAAAATGGTTCACGCT
Hs9	BIRC5 FWD	AGGACCACCGCATCTCTACAT
Hs10	BIRC5 RVS	AAGTCTGGCTCGTTCTCAGTG
Hs11	AFP FWD	CTTTGGGCTGCTCGCTATGA
Hs12	AFP RVS	GCATGTTGATTTAACAAGCTGCT
Hs13	ITGB2 FWD	AAGTGACGCTTTACCTGCGAC
Hs14	ITGB2 RVS	AAGCATGGAGTAGGAGAGGTC
Hs15	SERPINE1 FWD	TAGACCGATTATTGACCGACCT
Hs16	SERPINE1 RVS	GTTTGCCACGAGAATCAAATCC
Hs17	AXIN2 FWD	CAACACCAGGCGGAACGAA
Hs18	AXIN2 RVS	GCCCAATAAGGAGTGTAAGGACT
Hs19	NKD1 FWD	GGGAAACTTCACTCCAAGCC
Hs20	NKD1 RVS	CTCCCGATCCACTCCTCGAT
Hs21	SOX2 FWD	TACAGCATGTCCTACTCGCAG
Hs22	SOX2 RVS	GAGGAAGAGGTAACCACAGGG
Hs23	SNAI2 FWD	CGAACTGGACACACATACAGTG
Hs24	SNAI2 RVS	CTGAGGATCTCTGGTTGTGGT
Hs25	BIRC2 FWD	AGCACGATCTTGTCAGATTGG
Hs26	BIRC2 RVS	GGCGGGGAAAGTTGAATATGTA
Hs27	YAP1 FWD	TAGCCCTGCGTAGCCAGTTA
Hs28	YAP1 RVS	TCATGCTTAGTCCACTGTCTGT
Hs29	TAZ FWD	CACCGTGTCCAATCACCAGTC
Hs30	TAZ RVS	TCCAACGCATCAACTTCAGGT
Hs31	TEAD1 FWD	ATGGAAAGGATGAGTGACTCTGC
Hs32	TEAD1 RVS	TCCCACATGGTGGATAGATAGC
Hs33	LATS1 FWD	AAACCAGGGAATGTGCAGCAA
Hs34	LATS1 RVS	CATGCCTCTGAGGAACTAAGGA
Hs35	MST1 FWD	AAGCCGCAGTTCACGTTTAC
Hs36	MST1 RVS	GGGTCCATCGTGTAGCACC
Hs37	CTNNA1 FWD	GGGGATAAAATTGCGAAGGAGA

Hs38	CTNNA1 RVS	GTTGCCTCGCTTCACAGAAGA
Hs39	CDH1 FWD	CGAGAGCTACACGTTCACGG
Hs40	CDH1 RVS	GGGTGTCGAGGGAAAAATAGG
Hs41	YWHAZ FWD	CCTGCATGAAGTCTGTAACTGAG
Hs42	YWHAZ RVS	GACCTACGGGCTCCTACAACA

Gabriella C. Russo

3700 N. Charles St., Apt 107, Baltimore, MD 21218 | (732) 859-8296 |
gabriellarusso17@gmail.com

EDUCATION

The Johns Hopkins University
Masters of Science in Engineering in Chemical and Biomolecular Engineering, expected completion date May 2018
Bachelor of Science in Chemical and Biomolecular Engineering, May 2017

- **Cumulative GPA:** 3.3
- **Awards**: Dean's List Fall 2016 and Spring 2017
- **Relevant Coursework**: ChemBE Senior Lab, Kinetic Processes, Chemical and Biological Processes, Modeling Dynamics and Controls, Biochemistry, Organic Chemistry I, Cellular Biology

TECHNICAL SKILLS

Software: Microsoft Excel, GraphPad, MatLab, Microsoft PowerPoint, AutoCAD, Mathematica
Lab Skills: qPCR, 3D and 2D cell culture for both cell migration and drug response/efficacy, Western Blots, SDS-PAGE, immunofluorescence microscopy, bacterial cultures, *in vivo* mouse model experience

EXPERIENCE

Wirtz Lab **Baltimore, MD**
Graduate Research Assistant/Laboratory Technician June 2017- August 2017

- Developed protocols to run 384-well qPCR experiments to screen for target genes in triple negative breast cancer cells with Dr. MengHorng Lee.
- Utilized results from qPCR experiments to test inhibitors on triple negative breast cancer cells in both 3D layered tumor spheroid system and in 2D culture to analyze the differences in both methods.
- Analyzed data sets in both Excel and GraphPad to present data to my mentor and P.I. Dr. D.Wirtz.

Undergraduate Research Assistant January 2014 – May 2017

- Developed protocols for 2D cell culture experiments to measure the cell fold increase.
- Analyzed data in both Excel and GraphPad to generate useful models of the data to present to my mentor.
- Worked with Anjil Giri and Ivie Aifuwa on their projects in the migration of cancer cells by looking at specific proteins and their expression levels in normal and metastatic cells. Currently working with Dr. MengHorng Lee on 2D cell culture experiments to determine the effect of a cancer drug on the cell growth rate of two known cancer cell lines.

Streamline Tutors **Baltimore, MD**
SAT/ACT Tutor May 2017 – Present
Prepared students for college entrance exams by teaching the problem-solving skills and strategic test taking methods.

Department of Chemical and Biomolecular Eng. **Baltimore, MD**
Graduate Teaching Assistant August – December 2017
Assisted faculty to organize experiments and troubleshoot during the lab periods.

Office of Academic Advising Study Consultant **Baltimore, MD**
Study Consultant January 2016 – May 2017

- Mentored students on a weekly basis throughout the semester to help them develop better organizational skills, time management methods, and study habits.

EXTRA CURRICULARS

Johns Hopkins University Club Soccer **Baltimore, MD**
Member of the JHU Women's Team September 2013-May 2017